The Canadian Mineralogist
Vol. 47, pp. 107-128 (2009)
DOI: 10.3749/canmin.47.1.107

EXSOLUTION MICROSTRUCTURES IN NH_4-BEARING MUSCOVITE AND ANNITE IN GNEISSES FROM THE TORROX AREA, BETIC CORDILLERA, SPAIN

MARIA DOLORES RUIZ CRUZ§

Departamento de Química Inorgánica, Cristalografía y Mineralogía, Facultad de Ciencias, Universidad de Málaga, E–29071 Málaga, Spain

CARLOS SANZ DE GALDEANO[2]

Instituto Andaluz de Ciencias de la Tierra, CSIC – Universidad de Granada, Facultad de Ciencias, E–18071 Granada, Spain

ABSTRACT

Variably sized lamellae of annite within muscovite crystals and lamellae of muscovite within annite crystals from gneissic rocks of the Torrox area in the Betic Cordillera, Spain, are interpreted as formed by exsolution of NH_4-bearing micas present in the earliest metamorphic assemblage. The NH_4-rich white mica, identified only in the overlying schists, was formed during the first diagenetic-to-metamorphic episode, with N derived from the maturation of organic matter. Initially contained in white mica, the NH_4 was redistributed between white mica and annite, probably at conditions of increasing metamorphism. In the current assemblage of gneisses, NH_4 is preferentially concentrated in annite, especially in the composite Ms+Ann grains. This assemblage, which consists of muscovite in homogeneous grains + muscovite in exsolved grains + annite in homogeneous grains + annite in exsolved grains, was probably derived from the lower-temperature four-mica assemblage: muscovite + NH_4-rich white mica + annite + NH_4-bearing annite. Exsolution as temperature increased explains the presence of NH_4-rich micas in the overlying schists and the presence of exsolved grains in gneisses. The exsolution process occurred at ~450°C and ~3 kbar, physical conditions characterizing the first metamorphic episode affecting this formation.

Keywords: ammonium-rich mica, annite, Betic Cordillera, exsolution, muscovite, phengite, Spain.

SOMMAIRE

Nous interprétons la présence de lamelles d'annite de tailles différentes dans les cristaux de muscovite, et les lamelles de muscovite au sein des cristaux d'annite, dans les roches gneissiques de la région de Torrox, Cordillères Bétiques, en Espagne, en termes d'une exsolution de micas contenant NH_4 présents dans l'assemblage métamorphique précoce. Le mica blanc enrichi en NH_4, identifié uniquement dans les schistes de la séquence supérieure, a été formé au cours du premier épisode de recristallisation diagénétique à métamorphique, l'azote ayant été dérivé par maturation de la matière organique. Quoique initialement incorporé dans le mica blanc, le NH_4 fut redistribué entre mica blanc et annite probablement lors d'une augmentation du degré de métamorphisme. Dans l'assemblage actuel des gneiss, le NH_4 est de préférence incorporé dans l'annite, et surtout dans les grains composites à Ms + Ann. Cet assemblage, qui contient la muscovite en grains homogènes + la muscovite en grains exsolvés + l'annite en grains homogènes + l'annite en grains exsolvés, a probablement été dérivé à partir de l'assemblage à quatre micas stables à faible température: muscovite + mica blanc enrichi en NH_4 + annite + annite enrichie en NH_4. Une exsolution à mesure que la température a augmenté expliquerait la présence de micas riches en NH_4 dans les schistes de la séquence supérieure et la présence de grains exsolvés dans les gneiss. Le processus d'exsolution a eu lieu à environ 450°C et 3 kbar, conditions qui ont caractérisé le premier épisode métamorphique affectant cette formation.

(Traduit par la Rédaction)

Mots-clés: mica riche en NH_4, annite, exsolution, muscovite, phengite, Cordillères Bétiques, Espagne.

§ *E-mail address*: mdruiz@uma.es

Introduction

The term *exsolution* is generally applied to the formation of two separate phases, during cooling, from one homogeneous solid solution. Exsolution microstructures have been widely described in silicates, especially in feldspars, pyroxene and amphibole (Buseck *et al.* 1980, Ghose 1981, Robinson *et al.* 1982, Kretz 1994, and references therein) and are clear evidence of a miscibility gap between the exsolved phases. These structures are commonly observed in a petrographic microscope, but the descriptions of submicroscopic exsolution structures have considerably increased in recent decades as a consequence of the more generalized use of the transmission electron microscopy. Lamellae or rods formed through exsolution generally show clear topotactic relations with the host, and the interfaces have a preferred orientation.

Parallel or subparallel intergrowths of two different micas are very common. Nevertheless, the mechanisms responsible for these textures are generally topotactic nucleation of one mica on the other or, alternatively, hydrothermal alteration, whereas true exsolution intergrowths have been only rarely described (Ferrow *et al.* 1990, García-Casco *et al.* 1993, Ferraris *et al.* 2001).

The discovery of high-temperature NH_4-rich dioctahedral mica (tobelite) in most mica schists overlying the gneissic formations (Ruiz Cruz & Sanz de Galdeano 2008), and of a new NH_4-rich trioctahedral annite-like species (suhailite) in more restricted areas (Ruiz Cruz & Sanz de Galdeano 2009), led us to perform a detailed study of the gneissic rocks from the Torrox area, where a clear transition from schists to gneisses is observed, with two main objectives: 1) a test of the evolution of NH_4-bearing mica at the passage from the less metamorphosed schists to the more intensely metamorphosed gneissic formations, and 2) a detailed study of the composition of the several generations of micas in the gneissic rocks in order to establish their metamorphic evolution, taking into account the fact that ammonium-bearing micas had not been previously identified in these terranes. The NH_4-rich dioctahedral mica appears as scarce relics, widely replaced by muscovite and annite, and is characterized by high Fe+Mg contents, which are not coupled with a parallel increase in Si, characteristic of the phengitic micas. Suhailite appears as aggregates of golden mica grains unoriented with respect to the main foliation of the gneiss. Its average composition, as deduced from the analyses made at the scale of the scanning electron microscope, is: $[Ca_{0.04}Na_{0.07}K_{0.35}(NH_4)_{\Sigma 0.55}](Al_{0.42}Ti_{0.22}Fe_{1.33}Mn_{0.01}Mg_{0.71})(Si_{2.67}Al_{1.33})O_{10}(OH)_2$. Textural data indicate that unoriented grains of golden suhailite formed from primary reddish annite during the annite-to-"fibrolite" transformation.

Background Information

The solubility relationships among mica end-members are complex, and only some of the possible binary systems have been studied experimentally (*e.g.,* Flux *et al.* 1984, Monier & Robert 1986, Flux & Chatterjee 1986). Miscibility gaps have been found between the pair dioctahedral end-member (muscovite) and trioctahedral Mg–Fe end-member (phlogopite or annite). According to Monier & Robert (1986), this miscibility gap increases with increasing temperature. Muscovite solid-solutions can be expressed as the sum of the phengitic substitution (x) and the "biotitic" substitution (y). The general formula is: $K[Al_{2-x-2y/3}(Fe+Mg)_{x-y}\square_{1-y/3}](Si_{3+x}Al_{1-x})O_{10}(OH,F)_2$. The two parameters, x and y, allow one to estimate the approximate temperature of formation of a K-rich mica belonging to this chemical system. The influence of increasing pressure on the stability fields cannot be directly deduced from this diagram, although some approximations can be made using, in addition, the geobarometer of Massone & Schreyer (1987).

Ferraris *et al.* (2001) described exsolved lamellae of phlogopite in muscovite from a pegmatite of the central Alps. Using the composition of the host muscovite (x = 0.03, y = 0.12), they deduced that the temperatures of exsolution ranged between 600 and 650°C. On the other hand, from mass-balance calculations, they estimated the composition of the initial mica (x = 0.016, y = 0.17), and deduced that the crystallization temperature was ~500°C. This initial mica would have had an unusual composition, plotting near the di-trioctahedral join on the Monier & Robert diagram (very low extent of the phengitic substitution). These data clearly indicate that in contrast with the most common processes of exsolution, exsolution of phlogopite lamellae occurred during heating.

García-Casco *et al.* (1993) described a very similar example of biotite exsolution from white mica in gneisses from the Betic Cordillera. These authors deduced that muscovite would be equilibrated at 600–650°C, and P was of the order of 11 kbar; therefore, for the cited authors, exsolution would have occurred during rapid decompression, at near isothermal conditions. To Zeck & Whitehouse (1999), however, temperatures between 450 and 500°C and pressures of 12–13 kbar for the metamorphic climax are more likely to be correct.

Geological Setting

The Betic Cordillera has been traditionally divided into a northern external domain, including the Prebetic and the Subbetic zones, an intermediate domain, the Flysch units from the Gulf of Cádiz area, and a southern domain, the Internal Zone. Collision of the Internal and External zones during the Alpine orogeny (Upper Creta-

ceous to Miocene) caused intense structural deformation and metamorphism, which particularly affected the Internal Zone. Structurally, the Internal Zone is formed of four tectonically superimposed complexes, from the bottom upward, the Veleta and Mulhacén complexes, generally included in the Nevado–Filabride Complex, the Alpujárride and the Maláguide (Puga *et al*. 2002). The geotectonic relationships between the Maláguide, the Alpujárride and the Nevado–Filábride are essentially constant in the Betic Cordillera: the Maláguide complex tectonically overlies the Alpujárride complex, and this, in turns, overlies the Nevado–Filábride unit (Martín-Algarra 1987, Sanz de Galdeano 1997).

The Alpujárride complex shows sequences comprising poorly dated Paleozoic and probably older terranes and Triassic formations (Egeler & Simons 1969). The "Paleozoic" rocks are mainly schists, which evolve with depth toward gneisses or even migmatites. According to Azañón *et al*. (1997, 1998), and Booth-Rea *et al*. (2002), among others, both Triassic and Paleozoic rocks show an Alpine low-temperature – high-pressure metamorphism, overprinted by a high-temperature – low-pressure re-equilibration.

At the Torrox area, the upper Alpujárride unit consists of a large body of gneiss (~2.5 km^2) overlain by a thick sequence of graphite-rich mica schists. A description of the gneissic complex can be found in papers by García-Casco *et al*. (1993) and Zeck & Whitehouse (1999). In view of the strong deformation, the origin of the Torrox gneisses is still debated. Zeck & Whitehouse (1999) suggested that gneisses are derived from a granitic body of Hercynian age, although it should be noted that in some outcrops, there is a gradational contact between gneisses and the metapelitic schists.

Sampling and Methodology

From the initial study (unpubl. data) that revealed the presence of NH_4-mica in Alpujárride mica schists from Sierra Arana (area 7 in Fig. 1), a sampling of most outcrops of equivalent Alpujárride units was planned with the aim of investigating the extent of the distribution of NH_4-bearing mica throughout the Betic Cordillera. Nevertheless, in this paper, we deal only the results concerning the western part of the Torrox outcrop (Fig. 1, area 4), where a complete transition from gneisses to schists is exposed. In Table 1, we summarize the lithologies and mineralogical compositions of the samples studied.

A complete description of the methodology used can be found in Ruiz Cruz & Sanz de Galdeano (2008, 2009). Samples were systematically studied by petrographic microscopy, X-ray diffraction (XRD), Fourier transform infrared spectroscopy (FTIR), scanning electron microscopy (SEM), equipped with an

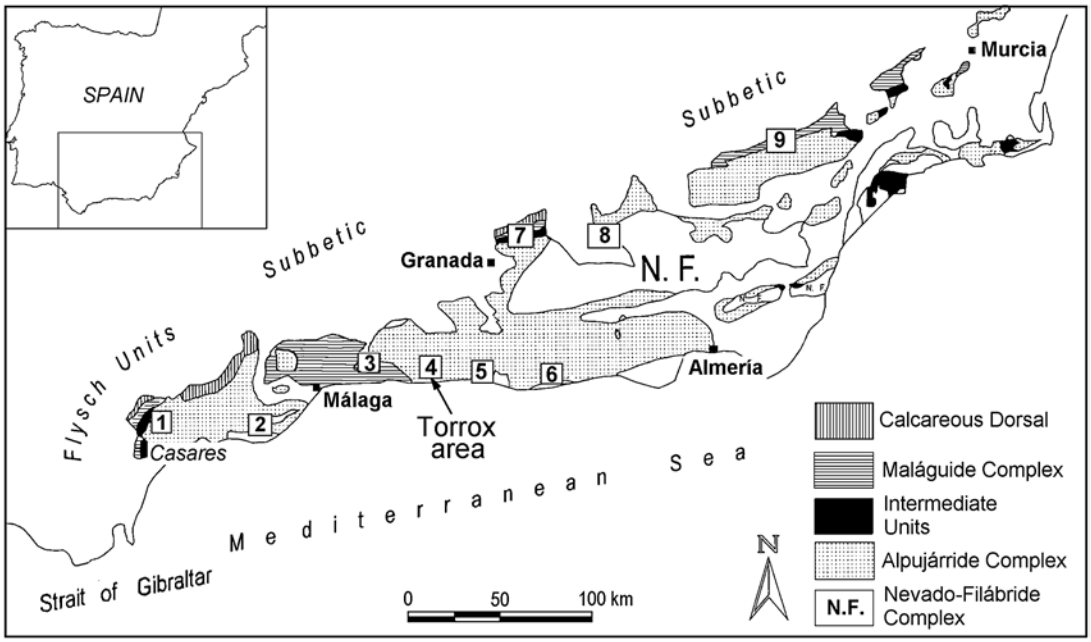

FIG. 1. Simplified geological map of the Betic Cordillera, Spain, showing the distribution of the Internal Zone Complexes, the position of the zones sampled, and the Torrox area (N 36°45'43.6", W 3°57'17.2").

X-ray energy-dispersive (EDS) system, and elemental analysis. Some selected samples were studied by transmission-analytical electron microscopy (TEM–AEM) and electron microprobe analysis (EMPA).

Randomly oriented samples were used for determination of the semiquantitative composition of minerals by XRD, and oriented samples were used for the quantification of the muscovite:annite ratio. This ratio was estimated from the relative intensity of the 003 reflections, after a previous calibration carried out with mixtures of muscovite and annite in several proportions.

Given the small size of the exsolved lamellae, commonly smaller than can be reliably determined by EMPA (10 μm), the samples were fist studied by scanning electron microscopy (SEM). Only some grains with an appropriate size were selected for the EMPA study. Obtaining of the EMPA data required a previous calibration of NH_4 using the two available standards (BN), supplied by Cameca and by Structure Probe, Inc. In addition, some grains of exsolved mica, also selected from thin sections, were ion-thinned for transmission-analytical electron microscopy (TEM–AEM) study. The abbreviation Ms includes muscovite and phengite, and we will use, in addition, N–M (for ammonium-rich white mica), and N–A (for ammonium-bearing annite). In all cases, given the presence of abundant graphite, mica formulae were calculated on the basis of $O_{10}(OH)_2$ and assuming Fe as Fe^{2+}.

Results

Sample description

Phase assemblages in all samples of gneisses studied are very similar. In addition to quartz, plagioclase and minor K-feldspar, the samples consist of mica (Ms and Ann), aluminosilicates (sillimanite and kyanite), staurolite, garnet, and very subordinate amounts of apatite, tourmaline, zircon, rutile and ilmenite. Retrograde phases are kaolinite and chlorite. The Ms:Ann ratio is very variable (from 65:35 to 25:75), as deduced from the XRD patterns. Muscovite crystals generally are medium- to coarse-grained (<1 to >5 mm). Two main types of Ms can be differentiated: a) large, slightly deformed grains (primary metamorphic Ms, after García-Casco *et al.* 1993), which generally maintain the orientation of the foliation, and b) large but undeformed and randomly oriented grains (pegmatitic Ms, after García-Casco *et al.* 1993). Primary Ms includes, in addition, two types of grains: uniform grains and grains containing abundant Ann lamellae parallel to the cleavage planes in Ms (Figs. 2A, B). These latter grains show a characteristic exsolution-induced texture, previously described by García-Casco *et al.* (1993). The size and the number of Ann lamellae are very variable from grain to grain. The mean Ms:Ann ratio, as deduced from an image analysis of more that 50 grains, is 1:2.6 (by weight). Both types of primary Ms grains appear to be contemporary and are postdated by kyanite (Fig. 2C). Late Ms grains show an advanced retrogression to kaolinite (Fig. 2B).

TABLE 1. TYPE AND LOCATION OF THE NH_4-BEARING SAMPLES STUDIED

Sample	Lithology	Main assemblage of minerals
MP-2	Light banded gneiss	Qtz + Pl + Kfs + Ms + Ann + Ky + Sil + St + Grt
MP-3	Qtz-rich segregation	Qtz + Ann + Ms + (And)
MP-4	Ann-rich banded gneiss	Qtz + Kfs + (Pl) + Ms + Ann + And
MP-5	Light banded gneiss	Qtz + Pl + Kfs + Ms + Ann + (Ky) + (Sil) + St + Grt
MP-6	Light schist-gneiss	Qtz + Pl + Ms + Ann + Ky + Grt
MP-7	Light mica schist	Qtz + Pl + Ms + Ann + N-M + (Ky) + (Sil) + St + Grt
MP-8	Dark mica schist	Qtz + Pl + Ms + Ann + Ky + Tob + (Sil) + St + Grt

N-M: Ammonium-rich white mica.

Most grains of Ann show a homogeneous aspect, as observed by optical microscopy (Fig. 2A). Nevertheless, some other grains contain abundant inclusions of graphite and rutile (Figs. 2A,D). Annite appears replaced by sillimanite to a variable extent.

The back-scattered electron images (BSE) also reveal some significant features. For example, graphite-rich Ann grains commonly contain micro- to nanometric lamellae of Ms showing a disk-shaped form, typical of some exsolution textures in micas (Veblen 1983), which were not identified by optical microscopy (Fig. 3A). It is thus evident that the exsolution processes affected both Ann and Ms grains, although the style of exsolution was clearly different. Annite lamellae included in Ms are generally euhedral, and the contact between the two micas is generally planar (Fig. 3B). In contrast, Ms lamellae included within Ann show generally curved boundaries, and interfaces perpendicular to the basal planes are lacking (Fig. 3A). The estimation of the Ms:Ann ratio in these Ann-rich grains is hindered by the presence of areas with intermediate contrast and by the form of the Ms lamellae. The chemical profiles carried out on these grains (see below) suggest that this ratio is ~1:3 (by weight).

Samples of schist show, in contrast with samples of gneiss, a notably higher mica content, although a clear gradation in texture and mica content, mainly represented by sample MP–6, is evident. They contain similar metamorphic assemblages, including kyanite, sillimanite, garnet and, in some cases, abundant andalusite. Large grains of staurolite are characteristic of some schist samples (*e.g.*, MP–8). Exsolution textures were not observed in mica grains in schists, although they contain abundant subparallel intergrowths of Ms and Ann. In addition to Ms, the schists (samples MP–7 and MP–8) contain relics of graphite-rich N–M, similar to that found in other areas and described in a previous paper (Ruiz Cruz & Sanz de Galdeano 2008). Nevertheless, N–M is very scarce in these rocks, because it

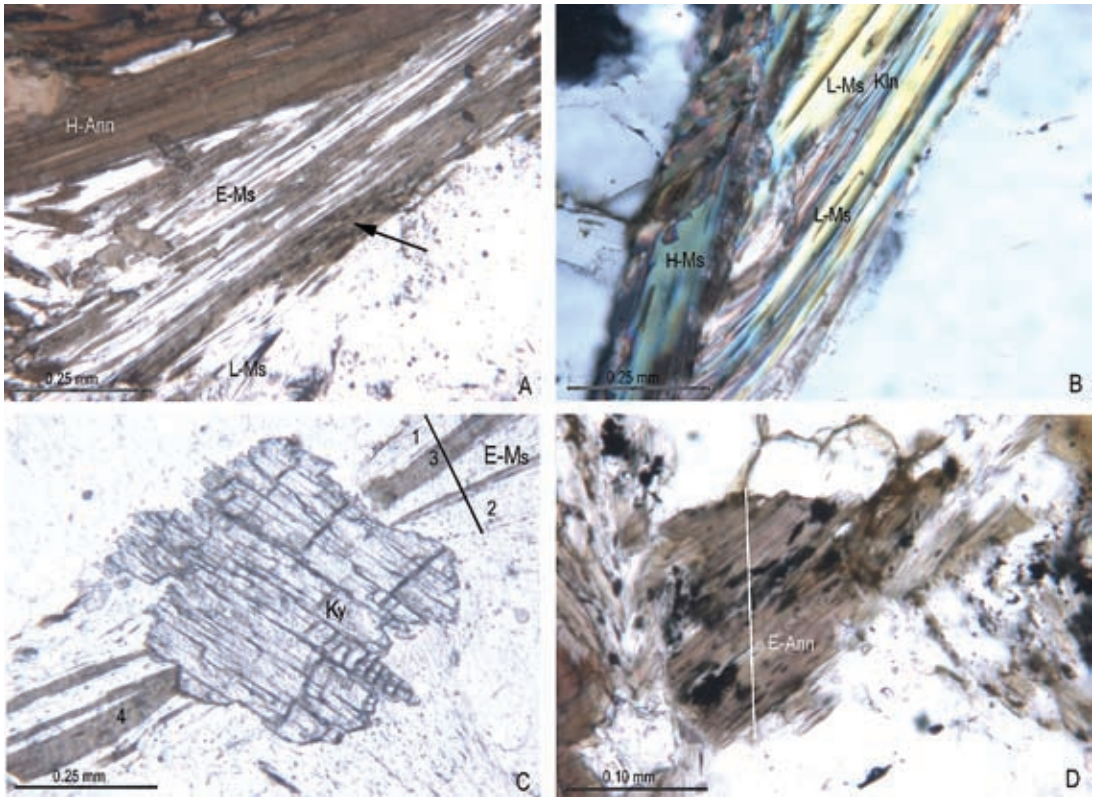

FIG. 2. Representative optical microscope images of micas from gneisses and schists. A) Muscovite grain with exsolved Ann lamellae (E–Ms), homogeneous Ann grain (H–Ann), and annite with abundant rutile and graphite inclusions (arrow) from sample MP–2 (parallel nicols). B) Homogeneous Ms grain (H–Ms), partially replaced by late Ms (L–Ms), extensively retrograded to kaolinite (Kln) from sample MP–2 (crossed nicols). C) Kyanite grain postdating the primary exsolved Ms grains (E–Ms) from sample MP–5 (parallel nicols). Numbers correspond to EMPA analyses in Table 8, and the black line, to the profile shown in Figure 13A. D) Graphite-rich Ann grain (E–Ann) from sample MP–2 (parallel nicols). The white line corresponds to the profile shown in Figure 13B.

seems to have been extensively replaced by Ms and Ann. Back-scattered images permit the easy identification of N–M, which shows characteristic fractures, and a contrast intermediate between that of muscovite and that of kaolinite (Fig. 3C). Schists also contain two texturally different types of Ann: Ann grains intergrown with Ms, defining the main schistosity, and smaller grains of Ann included in kyanite (Fig. 3D).

The ammonium content of the micas

Identification of N–M was firstly based on the presence of a basal reflection with a spacing greater than 10 Å in the XRD patterns (Higashi 1982, Drits *et al*. 1997), although in most cases, owing the low N–M content relative to Ms and Ann, deconvolution of the more intense peak of mica (10 Å) was necessary to unambiguously detect the presence of N–M. The presence of NH_4 in our samples was confirmed by infrared spectroscopy; all the samples studied show a weak but characteristic 1430 cm^{-1} band (Chourabi & Fripiat 1981, Busigny *et al*. 2003). In addition, a more precise determination of the NH_4 content was carried out by elemental analysis (Shigorova *et al*. 1981, Schroeder & Ingall 1994, Schroeder & McLain 1998).

In Table 2, we summarize the C and N contents determined in mica-enriched separates or in whole-rock samples, as well as the calculated NH_4 contents in mica. The estimated values represent, however, mean values, assuming a homogeneous distribution of NH_4 in all populations of mica present in the rocks, which is not the case. The values obtained in some samples of gneisses are higher than those determined in NH_4-enriched biotite from metamorphic rocks (Duit

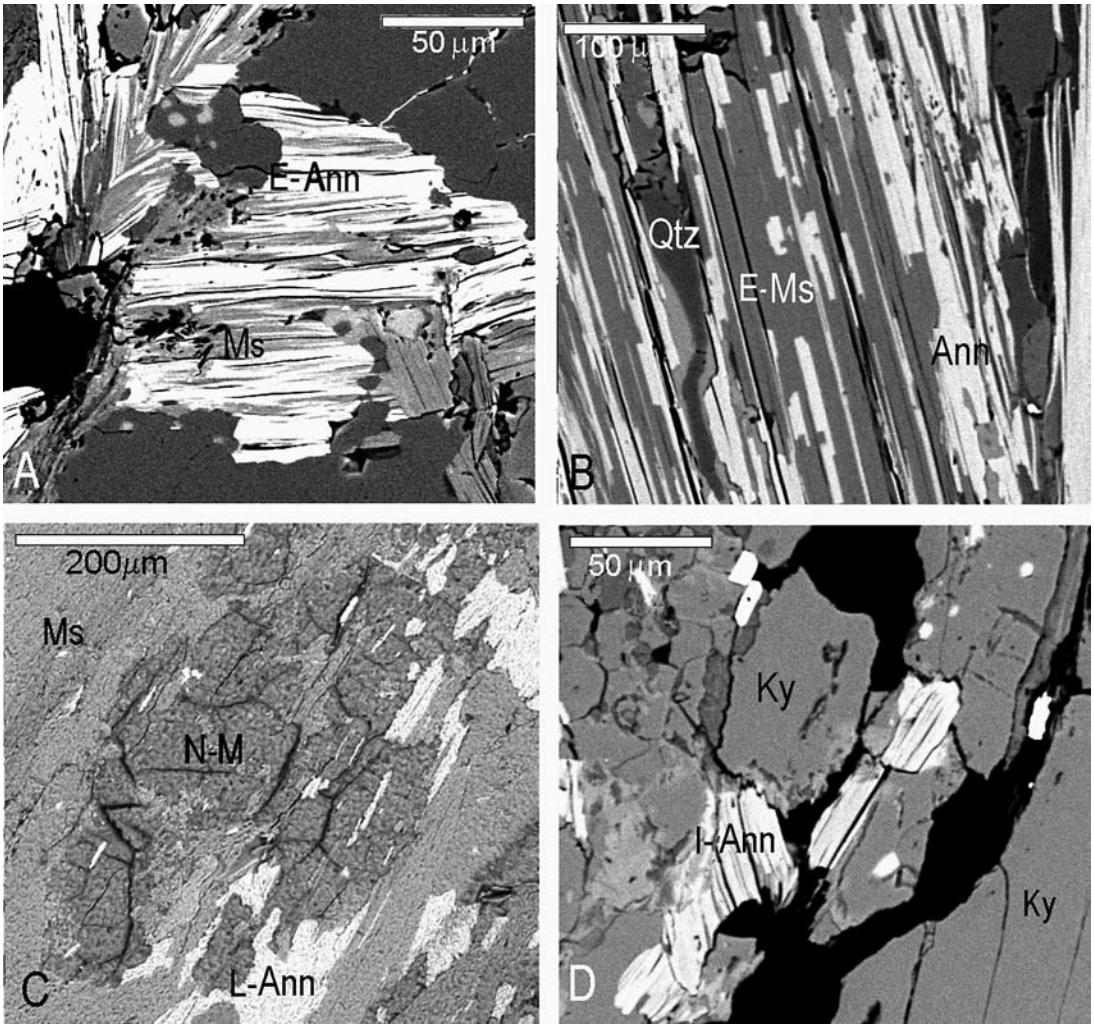

FIG. 3. Back-scattered electron images of micas. A) Ann grain from Figure 2D, showing the morphology of the Ms lamellae intergrown with Ann. B) Ms grain (Fig. 2A) with abundant lamellae of Ann, showing a characteristic style of exsolution. C) Relics of ammonium-rich white mica (N–M) extensively replaced by Ms and Ann, and showing characteristic fractures (sample MP–8). D) Small Ann grains included within kyanite (sample MP–7).

et al. 1986, Boyd & Philippot 1998, Mingram & Braüer 2001). The values measured in schists are slightly lower, although contents of up to 0.70 wt.% have been determined in mica from areas near the Torrox outcrop (area 5 in Fig. 1). No clear correlation between rock type or dominant type of mica and NH_4 content is evident from these data.

The composition of the micas

Representative results of SEM–EDS analyses of micas are reported in Tables 3–6. Chemical data for Ms from gneisses have been graphically represented in Figure 4. The several textural types of Ms define almost continuous compositional trends, as also noted by García-Casco *et al*. (1993). The average formulae deduced for primary Ms (homogeneous and exsolved), Ms lamellae exsolved in Ann grains, and late Ms are reported in Table 7 (formulae 1–4).

Primary homogeneous Ms and Ms from composite Ms + Ann lamellae show rather similar compositions. More notable differences are observed between primary and late Ms. These include a decrease of Si, the parallel increase of total Al (Fig. 4A) and a decrease

TABLE 2. BULK C AND N CONTENTS IN WHOLE ROCKS OR MICA CONCENTRATES, AND NH_4 CONTENTS DEDUCED FOR MICA

	C	N	Mica	N*	NH_4*	Ms:Ann ratio
			Gneisses			
MP-2	0.713	0.043	20	0.22	0.28	50:50
MP-3	0.182	0.056	80	0.07	0.09	90:10
MP-4	0.772	0.054	93	0.06	0.07	25:75
MP-5	0.681	0.062	30	0.21	0.27	35:65
			Schists			
MP-6	0.431	0.065	35	0.19	0.24	90:10
MP-7	0.395	0.067	70	0.10	0.12	40:60
MP-8	0.601	0.089	50	0.13	0.17	25:75

NH_4* has been deduced assuming that N is contained in micas only and that it is homogeneously distributed in these. Concentrations are expressed in wt.%.

of the Fe + Mg content (Figs. 4B, C); all these changes lead to a near-ideal formula of Ms for the late grains, which probably favors the alteration to kaolinite. As a whole, Ms compositions define a phengitic trend, as indicated the positive correlation between Si and Fe + Mg (Fig. 4B).

In contrast with Ms, data in Table 4 and plots in Figure 5 reveal that Ann from composite Ms + Ann grains and homogeneous Ann grains define two different chemical trends, which are especially evident in the Fe + Mg *versus* Si (Fig. 5B), Na + K + Ca *versus* Si (Fig. 5D) and Na + K + Ca (or Si) *versus* Ti (not shown). Annite from homogeneous grains shows a uniform composition, characterized by high occupancy of the interlayer (~1.00 atoms per formula unit, *apfu*), and low Si and high Ti contents (formula 5 in Table 7). Annite from composite Ms + Ann grains is also compositionally homogeneous in both muscovite- and

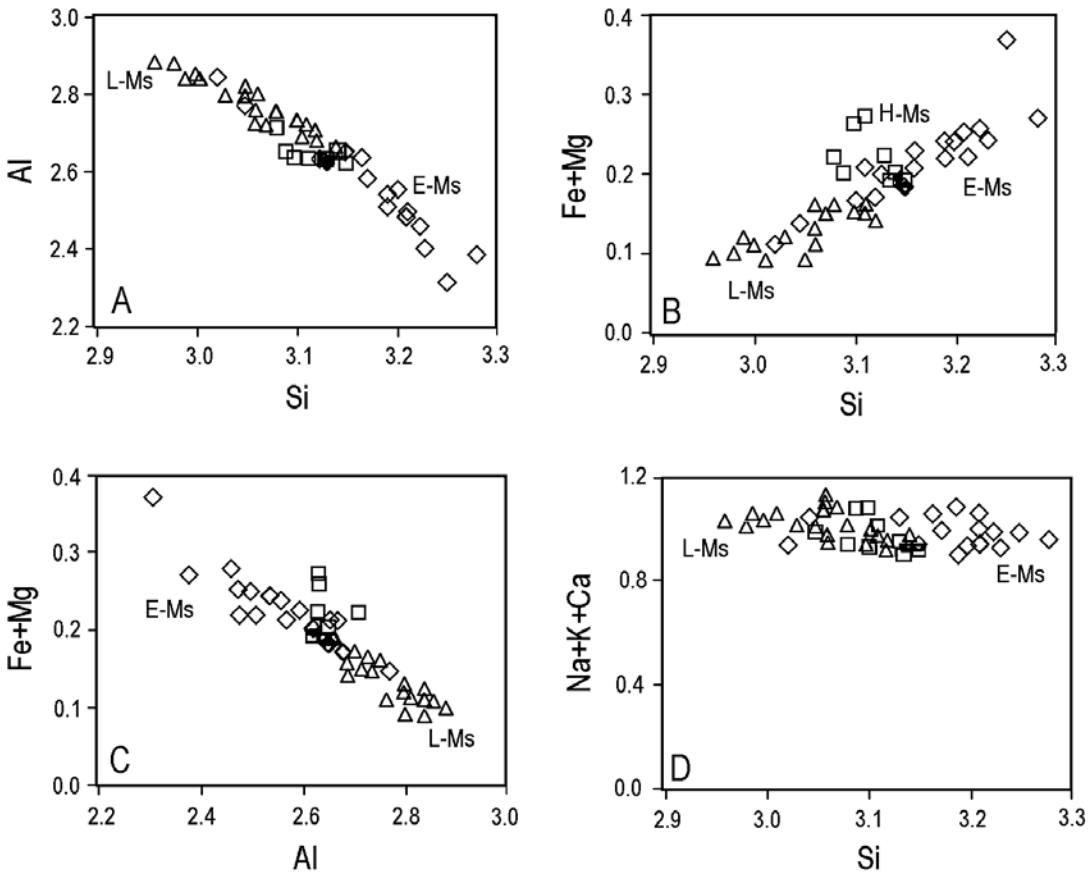

FIG. 4. Selected binary plots showing the most significant chemical characteristics of white micas from gneisses. Diamonds: muscovite grains with exsolved Ann lamellae and Ms lamellae exsolved in Ann. Squares: homogeneous, primary Ms. Triangles: late Ms.

TABLE 3. CHEMICAL COMPOSITION OF WHITE MICA FROM GNEISSES

	Ms host				Ms lamellae					Homogeneous Ms				Late Ms					
	1	2	3	Ave.	4	5	6	7	Ave.	8	9	10	Ave.	11	12	13	14	15	Ave.
SiO_2	44.35	45.74	47.13	45.74	45.69	46.99	48.29	49.80	47.25	46.21	46.88	47.67	46.92	45.44	45.14	45.94	45.81	45.03	45.52
Al_2O_3	33.92	32.42	30.91	32.42	32.93	32.30	31.67	30.56	31.91	33.60	33.26	31.84	32.90	36.73	36.14	36.11	35.71	34.14	35.80
TiO_2	0.86	0.93	1.00	0.93	0.64	0.90	1.17	1.16	0.93	1.20	0.96	1.07	1.08	1.08	1.00	1.10	1.10	0.35	0.93
Cr_2O_3	0.00	0.01	0.01	0.01	0.00	0.04	0.08	0.06	0.03	0.04	0.00	0.00	0.01	0.09	0.00	0.08	0.11	0.05	0.07
MnO	0.00	0.02	0.04	0.02	0.15	0.07	0.00	0.02	0.05	0.00	0.02	0.17	0.07	0.06	0.09	0.07	0.00	0.02	0.05
FeO	1.34	1.65	1.96	1.65	2.61	2.62	2.60	2.48	2.65	1.89	1.85	1.93	1.89	1.25	0.98	1.26	1.11	1.62	1.24
MgO	1.06	1.14	1.21	1.14	1.04	1.02	1.04	1.35	1.10	0.94	0.97	1.06	0.99	0.46	0.32	0.45	0.35	0.64	0.44
CaO	0.00	0.00	0.00	0.00	0.00	0.04	0.08	0.00	0.03	0.00	0.00	0.00	0.00	0.00	0.00	0.01	0.00	0.00	0.00
Na_2O	0.34	0.31	0.27	0.31	0.21	0.10	0.00	0.00	0.07	0.45	0.21	0.41	0.36	0.54	0.22	0.45	0.40	0.17	0.36
K_2O	11.20	11.18	11.36	11.23	11.35	11.46	11.57	11.37	11.57	10.98	11.19	11.23	11.13	11.03	11.68	11.15	11.23	10.97	11.22
Total	93.07	93.39	93.90	93.44	94.62	95.56	96.50	96.80	95.59	95.30	95.35	95.38	95.34	96.69	95.57	96.63	95.81	92.98	95.63
Si *apfu*	3.05	3.13	3.21	3.13	3.11	3.16	3.21	3.28	3.18	3.10	3.14	3.20	3.14	3.00	3.02	3.03	3.04	3.09	3.03
^{IV}Al	0.95	0.87	0.79	0.87	0.89	0.84	0.79	0.72	0.82	0.90	0.86	0.80	0.86	1.00	0.98	0.97	0.96	0.91	0.97
^{VI}Al	1.79	1.75	1.69	1.74	1.74	1.71	1.69	1.66	1.70	1.75	1.76	1.71	1.74	1.85	1.86	1.83	1.84	1.84	1.85
Ti	0.04	0.05	0.05	0.05	0.03	0.05	0.06	0.06	0.05	0.06	0.05	0.05	0.05	0.05	0.05	0.05	0.05	0.02	0.05
Mn	0.00	0.00	0.00	0.00	0.01	0.00	0.00	0.00	0.00	0.00	0.00	0.01	0.00	0.00	0.00	0.00	0.00	0.00	0.00
Fe	0.08	0.09	0.11	0.09	0.15	0.15	0.14	0.14	0.15	0.11	0.10	0.11	0.11	0.07	0.05	0.07	0.06	0.09	0.07
Mg	0.11	0.12	0.12	0.12	0.11	0.10	0.10	0.13	0.11	0.09	0.10	0.11	0.10	0.05	0.03	0.04	0.03	0.06	0.04
Σoct.	2.02	2.01	1.98	2.00	2.04	2.02	2.00	1.99	2.01	2.01	2.01	1.99	2.00	2.02	2.00	2.01	2.00	2.02	2.01
Ca	0.00	0.00	0.00	0.00	0.00	0.00	0.01	0.00	0.00	0.00	0.00	0.00	0.00	0.00	0.00	0.00	0.00	0.00	0.00
Na	0.05	0.04	0.04	0.04	0.03	0.01	0.00	0.00	0.01	0.06	0.03	0.05	0.05	0.07	0.03	0.06	0.05	0.02	0.05
K	0.98	0.98	0.99	0.98	0.98	0.98	0.98	0.96	0.99	0.94	0.96	0.96	0.95	0.93	0.99	0.94	0.95	0.96	0.95
Na+K +Ca	1.03	1.02	1.02	1.02	1.01	0.99	0.99	0.96	1.00	1.00	0.98	1.01	1.00	1.00	1.02	1.00	1.00	0.98	1.00

The compositional data, acquired by energy-dispersion spectrometry, are reported in wt.%.

annite-exsolved grains. It is characterized by higher Si and Al contents (Fig. 5A), coupled with very low Ti contents and low occupancy of interlayer (~0.55 *apfu*). The chemical trends (the increase of Si, Al, Fe and Mg) clearly indicate that the low charge of the interlayer is not due to contamination by chlorite or kaolinite; it seems evident that the NH_4 content is high in these Ann grains. On the basis of this assumption, two formulae (6a–6b and 7a–7b) are presented in Table 7, the second set including NH_4 in the interlayer. As discussed in a previous paper (Ruiz Cruz & Sanz de Galdeano 2008), the second set of formulae was calculated on the basis of $O_{10}(OH)_2$, and assuming an interlayer occupancy of 1 *apfu*. The strong negative correlation between NH_4 content and Ti (not shown) confirms the microscope observations of the presence of abundant precipitates of rutile in these grains and suggests that Ti was expelled from the structure of the NH_4-enriched Ann.

White micas from schists (Ms and N–M) show clear chemical differences (Table 5) and chemical trends (Fig. 6), this despite the fact that the number of N–M analyses made is low. Muscovite shows an average chemical composition with limited phengitic substitution (Table 7, formula 8), although some variations in Si and Al contents are evident in Figure 7A. The NH_4-bearing dioctahedral mica has a mean composition (Table 7, formula 9b) slightly different from the average formulae (Table 7, formula 9c) deduced for N–M from other localities (Ruiz Cruz & Sanz de Galdeano 2008), being characterized by higher Fe + Mg contents (Figs. 6B, C) and higher octahedral-site occupancy.

Two populations are also evident in Figure 7 and Table 7 for Ann from schists. One corresponds to the small Ann grains included within kyanite (Fig. 3D), which probably represent the older generation of annite. This population is characterized by low Na + K + Ca contents (~0.75 *apfu*), suggesting that the interlayer is partially occupied by NH_4 (Table 7, formula 10a–10b). The octahedral-site occupancy (2.63 *apfu*) indicates, in addition, that this population of Ann has an important dioctahedral component, similarly to Ann described by Pichavant *et al.* (1988). The other population is characterized by lower Si and Al contents and higher Fe + Mg contents, and corresponds to the more abundant Ann grains, parallel to the main schistosity (Table 7, formula 11).

We have also obtained some chemical data of the several populations of mica by EMPA. These analyses are hindered by the rapid volatilization of NH_4, although this effect is considerably less pronounced in Ann than in the dioctahedral mica (Ruiz Cruz & Sanz de Galdeano 2008, 2009). Results of some analyses of Ms and Ann, obtained in grains with coarse lamellae of Ann (grains shown in Fig. 2C), are reported in Table 8. The EMPA-derived formulae indicate, as do the data obtained at the SEM scale for thinner lamellae, that ammonium is concentrated in Ann. Given the small size of the Ms lamellae exsolved in the Ann grains, EMPA examination of these grains invariably provided mixed compositions of Ms and Ann.

TEM–AEM data

Grains of mica from gneiss samples with exsolution structures have also been characterized by TEM–AEM. The low-magnification images of the Ms grains containing Ann lamellae confirm the optical and SEM observations, indicating that Ann lamellae show planar boundaries with the host Ms (Fig. 8). The lattice-fringe images reveal, however, that the boundaries between the two phases, coherent in appearance, are generally occupied by a thin packet (~150 Å) of a 7-Å phase that generally becomes amorphous during the analysis (Fig. 8, inset). Whereas the host Ms shows packets with apparent structural regularity, the exsolved lamellae of Ann contain a variety of structural defects, including terminations of one or more layers and lenticular gaps. The EDS spectra in Figure 8 reflect the lower K content in the Ann lamellae than in the host muscovite.

Although the mica grains were oriented before the high-resolution images were obtained, the different orientation of the mica packets only allowed us to obtain high-resolution images of some packets. Lattice-fringe images of Ms show scarce structural defects (Fig. 9A). The Ann lamellae show areas with high structural regularity (Fig. 9B) and areas consisting of subparallel packets with variable orientations, including thin amorphized packets (Fig. 9C). The Fourier-transform images (Fig. 9, inset) reveal that several packets of mica layers share the *c** axis only. The high-resolution image obtained along the [100] direction (Fig. 9C) reveals that the Ann packets show variable stacking sequences, including one- and two-layer polytypes. The Fourier-transform image (Fig. 9C, inset) shows, in addition to

TABLE 4. CHEMICAL COMPOSITION OF ANNITE FROM GNEISSES

	Ann host					Exsolved lamellae						Homogeneous Ann							
	1	2	3	4	Ave.	5	6	7	8	9	Ave.	10	11	12	13	14	15	16	Ave.
SiO_2	32.75	33.67	33.94	32.70	33.29	33.58	32.72	33.50	34.40	35.08	33.87	32.14	32.34	32.61	31.82	33.36	33.09	34.12	32.79
Al_2O_3	18.90	19.50	19.72	18.39	19.14	19.36	18.78	19.66	19.62	20.55	19.60	18.25	17.66	17.79	16.89	18.19	17.96	18.93	17.96
TiO_2	0.31	0.87	1.25	0.16	0.66	2.60	0.31	0.27	0.77	0.78	0.96	3.94	4.16	4.46	4.85	4.28	4.33	3.98	4.29
Cr_2O_3	0.00	0.00	0.04	0.00	0.01	0.01	0.10	0.07	0.00	0.00	0.04	0.10	0.00	0.10	0.04	0.02	0.12	0.09	0.06
MnO	0.31	0.35	0.27	0.32	0.31	0.27	0.42	0.32	0.27	0.34	0.32	0.26	0.32	0.27	0.22	0.29	0.15	0.21	0.25
FeO	27.92	27.18	26.40	28.07	27.39	21.94	26.99	26.68	25.95	23.81	26.26	24.59	24.37	23.96	23.45	23.51	23.69	22.50	23.74
MgO	6.27	6.32	5.84	5.91	6.08	6.34	6.88	7.01	6.34	5.83	6.15	5.27	5.49	5.19	4.82	5.34	4.95	5.63	5.24
CaO	0.23	0.17	0.23	0.24	0.22	0.15	0.30	0.20	0.22	0.21	0.21	0.08	0.00	0.00	0.10	0.09	0.01	0.23	0.07
Na_2O	0.39	0.05	0.29	0.00	0.18	0.14	0.05	0.12	0.00	0.00	0.06	0.09	0.08	0.02	0.11	0.09	0.00	0.21	0.09
K_2O	4.49	5.57	4.99	4.82	4.98	9.52	4.10	4.00	5.14	4.80	5.56	9.55	9.94	10.14	8.56	9.74	9.86	9.52	9.62
Total	91.57	93.68	92.96	90.60	92.27	93.90	90.64	91.83	92.71	91.39	93.04	94.26	94.32	94.56	90.88	94.92	94.16	95.41	94.11
Si *apfu*	2.65	2.66	2.68	2.68	2.67	2.64	2.66	2.67	2.71	2.76	2.68	2.57	2.59	2.60	2.62	2.63	2.63	2.65	2.61
^{IV}Al	1.35	1.34	1.32	1.32	1.33	1.36	1.34	1.33	1.29	1.24	1.32	1.43	1.41	1.40	1.38	1.37	1.37	1.35	1.39
^{VI}Al	0.46	0.47	0.51	0.46	0.48	0.44	0.46	0.51	0.53	0.66	0.50	0.29	0.26	0.27	0.26	0.32	0.32	0.38	0.30
Ti	0.02	0.05	0.07	0.01	0.04	0.15	0.02	0.02	0.05	0.05	0.06	0.24	0.25	0.27	0.30	0.25	0.26	0.23	0.26
Mn	0.02	0.02	0.02	0.02	0.02	0.02	0.03	0.02	0.02	0.02	0.02	0.02	0.02	0.02	0.02	0.02	0.01	0.01	0.02
Fe	1.89	1.79	1.74	1.93	1.84	1.44	1.83	1.78	1.71	1.57	1.74	1.64	1.63	1.60	1.62	1.55	1.58	1.46	1.58
Mg	0.76	0.74	0.69	0.72	0.73	0.74	0.83	0.83	0.75	0.68	0.72	0.63	0.65	0.62	0.59	0.63	0.59	0.65	0.62
Σoct.	3.14	3.08	3.04	3.14	3.10	2.80	3.18	3.16	3.05	2.98	3.05	2.83	2.81	2.78	2.79	2.77	2.76	2.74	2.78
Ca	0.02	0.01	0.02	0.02	0.02	0.01	0.03	0.02	0.02	0.02	0.02	0.01	0.00	0.00	0.01	0.01	0.00	0.02	0.01
Na	0.06	0.01	0.04	0.00	0.03	0.02	0.01	0.02	0.00	0.00	0.01	0.01	0.01	0.00	0.02	0.01	0.00	0.03	0.01
K	0.46	0.56	0.50	0.50	0.51	0.96	0.42	0.41	0.52	0.48	0.56	0.97	1.02	1.03	0.90	0.98	1.00	0.94	0.98
Na+K +Ca	0.54	0.58	0.57	0.53	0.56	0.99	0.46	0.44	0.54	0.50	0.59	0.99	1.03	1.03	0.93	1.00	1.00	0.99	1.00

The compositional data, acquired by energy-dispersion spectrometry, are reported in wt.%.

TABLE 5. CHEMICAL COMPOSITION OF WHITE MICA FROM SCHISTS

	Muscovite									Ammonium mica							
	1	2	3	4	5	6	7	8	Ave.	9	10	11	12	13	14	15	Ave.
SiO_2 wt.%	45.12	45.68	46.04	45.54	46.10	46.38	46.72	47.01	45.98	46.58	45.78	44.96	45.99	46.61	47.13	45.09	46.03
Al_2O_3	35.27	35.74	35.64	34.67	34.82	34.97	34.42	34.04	35.10	37.43	37.64	36.03	36.16	36.95	36.76	33.44	36.35
TiO_2	1.22	1.17	1.26	0.85	0.82	0.99	0.95	0.89	1.02	0.00	0.00	0.02	0.14	0.02	0.02	0.13	0.05
Cr_2O_3	0.06	0.04	0.05	0.00	0.06	0.00	0.03	0.05	0.04	0.00	0.00	0.00	0.00	0.00	0.00	0.00	0.00
MnO	0.04	0.02	0.01	0.03	0.07	0.00	0.01	0.00	0.02	0.00	0.08	0.05	0.01	0.03	0.02	0.00	0.03
FeO	1.30	1.18	1.23	1.21	1.14	1.47	1.23	1.29	1.26	5.16	5.18	4.85	5.75	4.99	4.59	4.40	4.98
MgO	0.50	0.39	0.46	0.74	0.55	0.62	0.63	0.66	0.57	3.06	2.62	3.01	2.79	2.73	2.85	1.66	2.67
CaO	0.00	0.00	0.00	0.01	0.02	0.00	0.00	0.05	0.01	1.17	0.94	1.10	1.09	1.13	0.88	0.61	0.99
Na_2O	0.27	0.15	0.17	0.38	0.17	0.19	0.25	0.41	0.25	0.29	0.00	0.30	0.12	0.10	0.11	0.31	0.18
K_2O	11.51	11.19	11.25	11.36	11.61	10.76	11.48	11.76	11.37	0.14	0.15	0.18	1.01	0.14	0.44	7.18	1.33
Total	95.29	95.57	96.12	94.79	95.36	95.38	95.72	96.15	95.62	93.84	92.40	90.50	93.06	92.70	92.81	92.81	92.61
Si *apfu*	3.03	3.04	3.05	3.07	3.08	3.09	3.11	3.12	3.07	3.02	3.01	3.02	3.03	3.05	3.07	3.03	3.04
^{IV}Al	0.97	0.96	0.95	0.93	0.92	0.91	0.89	0.88	0.93	0.98	0.99	0.98	0.97	0.95	0.93	0.97	0.96
^{VI}Al	1.82	1.85	1.83	1.82	1.83	1.83	1.81	1.79	1.82	1.87	1.92	1.87	1.84	1.89	1.90	1.88	1.87
Ti	0.06	0.06	0.06	0.04	0.04	0.05	0.05	0.04	0.05	0.00	0.00	0.00	0.01	0.00	0.00	0.00	0.00
Mn	0.00	0.00	0.00	0.00	0.00	0.00	0.00	0.00	0.00	0.00	0.00	0.00	0.00	0.00	0.00	0.00	0.00
Fe	0.07	0.07	0.07	0.07	0.06	0.08	0.07	0.07	0.07	0.28	0.28	0.27	0.32	0.27	0.25	0.28	0.28
Mg	0.05	0.04	0.05	0.07	0.05	0.06	0.06	0.06	0.06	0.30	0.26	0.30	0.27	0.27	0.28	0.28	0.26
Σoct.	2.01	2.01	2.01	2.00	1.99	2.02	1.99	1.97	2.00	2.45	2.46	2.45	2.43	2.44	2.43	2.44	2.41
Ca	0.00	0.00	0.00	0.00	0.00	0.00	0.00	0.00	0.00	0.08	0.07	0.08	0.08	0.08	0.06	0.07	0.07
Na	0.03	0.02	0.02	0.05	0.02	0.03	0.03	0.05	0.03	0.04	0.00	0.04	0.02	0.01	0.01	0.02	0.02
K	0.99	0.95	0.95	0.98	0.99	0.91	0.97	1.00	0.97	0.01	0.01	0.02	0.08	0.01	0.04	0.03	0.11
Na+K+Ca	1.02	0.97	0.97	1.03	1.01	0.94	1.01	1.05	1.00	0.13	0.08	0.13	0.18	0.10	0.11	0.12	0.20

The compositional data were acquired by energy-dispersion spectrometry.

the Ann reflections, 7-Å reflections corresponding to the damaged areas. We do not know the chemical composition of this phase, since the packets are very small and the EDS spectra obtained of these areas (Fig. 8, inset) do not show clear variations in relation to those obtained in areas free of the 7-Å layers. This finding suggests that the 7-Å packets have a trioctahedral nature, probably berthierine- or amesite-like. Whether this phase is a subproduct of the exsolution process or of retrograde alteration of Ann also remains uncertain on the basis of the data available.

Although the low-magnification TEM images of the exsolved Ann grains suggest the presence of parallel boundaries between the host Ann and the exsolved Ms lamellae (Fig. 10), the lattice-fringe images reveal the presence of an array of interface dislocations approximately 200 Å apart (Fig. 11), which lead, at the scale of the optical images, to curved boundaries. In addition, the low-magnification images also show the presence of large inclusions of Fe oxide in the Ms lamellae. The EDS spectra of Ms are generally "contaminated" (Fig. 10, inset). Figure 11 also shows a Ms–Ann boundary oblique to the layers. The transition between the two phases occurs through a strongly damaged area.

The lattice-fringe images of host Ann show generally uniform 10-Å periodicity (Fig. 11). Nevertheless, small areas with regular 10 + 7 Å sequences (Fig. 12A), also revealed by the Fourier-transform image (Fig. 12A, inset), have been observed occasionally. Again, given the small size of these areas, the EDS spectra do not show obvious differences from those characterizing the 10-Å annite areas, suggesting that the 7-Å layers have a trioctahedral character. The high-resolution images of the exsolved Ms lamellae show bent layers, which prevent the accurate determination of the polytype. The image in Figure 12B reveals, however, the local presence of one- and two-layer sequences.

Two different styles of exsolution

Images in Figure 3 (A and B) clearly reveal two different styles of exsolution microstructures in Ms and Ann grains. Annite lamellae exsolved in Ms show generally planar boundaries, parallel to important crys-

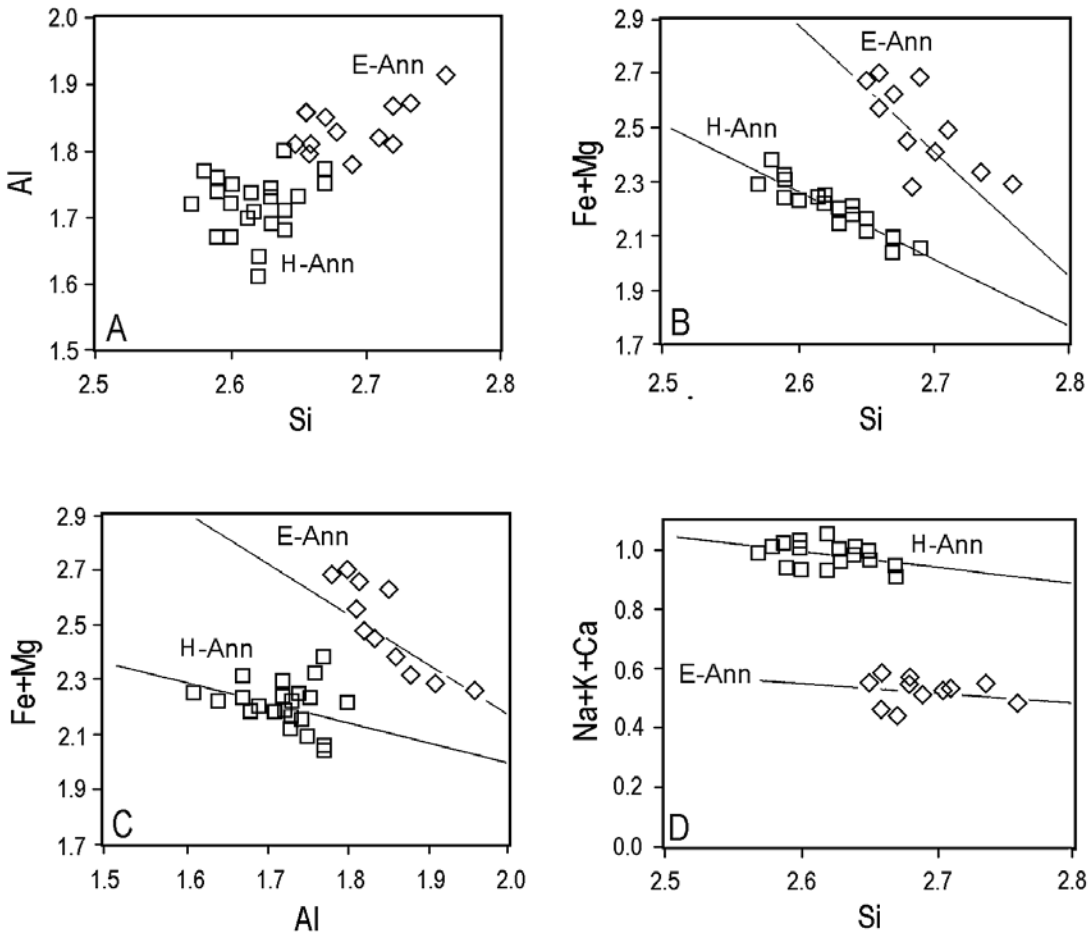

FIG. 5. Selected binary plots showing the most significant chemical characteristics of Ann from gneisses. Diamonds: annite grains with exsolved Ms lamellae and Ann lamellae exsolved in Ms. Squares: homogeneous Ann grains. In this and the following figures, the regression lines were drawn with Excel.

tallographic faces [(001) and (*hk*0)], similar to those observed in some pyroxene and amphibole crystals (*e.g.* Robinson *et al*. 1977, Buseck *et al*. 1980). In addition, they show sharp boundaries between phases, evident from the contrast in the BSE image. Exsolved lamellae of muscovite in Ann grains display, on the contrary, disk-shaped morphologies, and the (*hk*0) faces are lacking. In addition, gradual changes in contrast lead to a "modulated" aspect.

Confirmation of these SEM–BSE observations is evident in compositional profiles obtained across the two types of grains (Fig. 13), especially in the changes in Fe, Mg and Al through the grains. In the case of the exsolved Ms grains (Fig. 13A), these profiles reveal: 1) sharp variations in Mg, Al, and Fe at the boundaries between host Ms and Ann lamellae, 2) a small depletion in Mg and Fe, coupled with a slight increase of Al in the Ms areas near the Ann lamellae (1, in Fig. 13A), 3) higher and homogeneous K contents in Ms than in Ann lamellae, and 4) the presence of very thin lamellae of quartz, not observed optically (2, in Fig. 13A). The exsolved Ann grain (Fig. 13B) shows very different chemical profiles. These differences include: 1) a notably more tooth-shaped profile, which is due to various factors such as the smaller size of the Ms lamellae, the presence of graphite-rich areas (1, in Fig. 13B), and the less well-defined compositional boundaries between both types of micas, 2) a K content of the Ann host lower than that in the Ann lamellae of the exsolved Ms grain (2, in Fig. 13B), 3) an apparent

TABLE 6. CHEMICAL COMPOSITION OF ANNITE FROM SCHISTS

	Early						Late						
	1	2	3	4	5	Ave.	6	7	8	9	10	11	Ave.
SiO_2 wt.%	35.87	35.84	37.41	37.54	37.32	37.12	33.88	34.59	34.79	34.66	34.98	34.94	34.90
Al_2O_3	20.19	19.15	20.63	20.42	20.18	20.31	18.94	18.89	18.71	17.43	18.22	17.76	18.57
TiO_2	3.13	3.76	3.75	3.51	3.08	3.45	3.59	4.01	3.55	4.37	3.58	3.53	3.79
Cr_2O_3	0.00	0.00	0.00	0.00	0.00	0.00	0.00	0.10	0.02	0.13	0.06	0.15	0.07
MnO	0.33	0.16	0.27	0.22	0.35	0.27	0.10	0.28	0.21	0.21	0.18	0.29	0.20
FeO	20.39	20.83	19.83	19.54	19.46	20.21	21.16	23.60	23.77	24.21	21.70	21.73	22.75
MgO	5.56	5.48	5.75	5.39	5.66	5.62	5.91	5.17	5.30	4.20	5.69	5.93	5.48
CaO	0.31	0.95	0.87	0.25	0.52	0.57	0.24	0.40	0.25	0.14	0.15	0.12	0.22
Na_2O	0.13	0.25	0.15	0.06	0.21	0.16	0.00	0.37	0.15	0.01	0.12	0.00	0.10
K_2O	7.70	5.83	5.42	8.44	7.03	7.02	9.84	6.77	8.66	9.65	9.32	10.02	9.23
Total	93.60	92.25	94.09	95.36	93.81	94.73	93.67	94.17	95.42	95.01	94.00	94.47	95.30
Si *apfu*	2.76	2.78	2.80	2.82	2.83	2.80	2.67	2.69	2.70	2.73	2.74	2.73	2.70
^{IV}Al	1.24	1.22	1.20	1.18	1.17	1.20	1.33	1.31	1.30	1.27	1.26	1.27	1.30
^{VI}Al	0.59	0.53	0.62	0.62	0.63	0.60	0.42	0.42	0.41	0.34	0.42	0.37	0.40
Ti	0.18	0.22	0.21	0.20	0.18	0.20	0.21	0.23	0.21	0.26	0.21	0.21	0.22
Mn	0.02	0.01	0.02	0.01	0.02	0.02	0.01	0.02	0.01	0.01	0.01	0.02	0.01
Fe	1.31	1.35	1.24	1.22	1.23	1.27	1.39	1.53	1.54	1.59	1.42	1.42	1.47
Mg	0.64	0.63	0.64	0.60	0.64	0.63	0.69	0.60	0.61	0.49	0.66	0.69	0.63
Σoct.	2.74	2.74	2.74	2.66	2.70	2.71	2.73	2.81	2.78	2.71	2.72	2.72	2.74
Ca	0.03	0.08	0.07	0.02	0.04	0.05	0.02	0.03	0.02	0.01	0.01	0.01	0.02
Na	0.02	0.04	0.02	0.01	0.03	0.02	0.00	0.06	0.02	0.00	0.02	0.00	0.01
K	0.75	0.58	0.52	0.81	0.68	0.67	0.99	0.67	0.86	0.97	0.93	1.00	0.91
Na+K+Ca	0.80	0.69	0.61	0.84	0.75	0.74	1.01	0.76	0.90	0.98	0.96	1.01	0.94

The compositional data were acquired by energy-dispersion spectrometry.

TABLE 7. MEAN CHEMICAL FORMULA OF THE SEVERAL TYPES OF MICA ENCOUNTERED

		Σ_{oct}	Σ_{inter}	
Gneiss samples				
Primary homogeneous muscovite (H-Ms)	$Na_{0.05}K_{0.95}(Al_{1.74}Ti_{0.05}Fe_{0.11}Mg_{0.10})(Si_{3.14}Al_{0.86})O_{10}(OH)_2$	2.00	1.00	(1)
Host muscovite (E-Ms)	$Na_{0.04}K_{0.98}(Al_{1.74}Ti_{0.05}Fe_{0.09}Mg_{0.12})(Si_{3.13}Al_{0.87})O_{10}(OH)_2$	2.00	1.02	(2)
Muscovite lamellae in annite (Ms)	$Na_{0.01}K_{0.99}(Al_{1.70}Ti_{0.05}Fe_{0.15}Mg_{0.11})(Si_{3.18}Al_{0.82})O_{10}(OH)_2$	2.03	1.01	(3)
Late muscovite (L-Ms)	$Na_{0.05}K_{0.95}(Al_{1.85}Ti_{0.05}Fe_{0.07}Mg_{0.04})(Si_{3.03}Al_{0.97})O_{10}(OH)_2$	2.01	1.00	(4)
Primary homogeneous annite (H-Ann)	$Ca_{0.01}Na_{0.02}K_{0.97}(Al_{0.30}Ti_{0.28}Fe_{1.56}Mn_{0.02}Mg_{0.62})(Si_{2.61}Al_{1.39})O_{10}(OH)_2$	2.78	1.00	(5)
Host annite (E-Ann)	$Ca_{0.02}Na_{0.03}K_{0.51}(Al_{0.48}Ti_{0.04}Fe_{1.84}Mn_{0.02}Mg_{0.73})(Si_{2.67}Al_{1.33})O_{10}(OH)_2$	3.10	0.56	(6a)
	$Ca_{0.02}Na_{0.01}K_{0.50}(NH_4)_{0.47}(Al_{0.397}Ti_{0.04}Fe_{1.80}Mg_{0.72})(Si_{2.62}Al_{1.38})O_{10}(OH)_2$	2.93	1.00	(6b)
Annite lamellae in muscovite (Ann)	$Ca_{0.02}Na_{0.01}K_{0.56}(Al_{0.50}Ti_{0.06}Fe_{1.74}Mn_{0.02}Mg_{0.72})(Si_{2.68}Al_{1.32})O_{10}(OH)_2$	3.05	0.59	(7a)
	$Ca_{0.02}Na_{0.01}K_{0.58}(NH_4)_{0.42}(Al_{0.42}Ti_{0.04}Fe_{1.71}Mg_{0.74})(Si_{2.63}Al_{1.37})O_{10}(OH)_2$	2.91	1.00	(7b)
Schist samples				
Muscovite (Ms)	$Na_{0.03}K_{0.97}(Al_{1.82}Ti_{0.05}Fe_{0.07}Mg_{0.06})(Si_{3.07}Al_{0.93})O_{10}(OH)_2$	2.00	1.00	(8)
Ammonium-rich white mica (N-M)	$Ca_{0.07}Na_{0.02}K_{0.11}(Al_{1.87}Fe_{0.28}Mg_{0.26})(Si_{3.04}Al_{0.96})O_{10}(OH)_2$	2.41	0.20	(9a)
	$Ca_{0.09}Na_{0.01}K_{0.11}(NH_4)_{0.79}(Al_{1.66}Ti_{0.01}Fe_{0.26}Mg_{0.25})(Si_{2.93}Al_{1.07})O_{10}(OH)_2$	2.19	1.00	(9b)
	$Ca_{0.09}Na_{0.01}K_{0.09}(NH_4)_{0.81}(Al_{1.72}Fe_{0.28}Mg_{0.12})(Si_{2.95}Al_{1.05})O_{10}(OH)_2$	2.13	1.00	(9c)
Annite included in kyanite (I-Ann)	$Ca_{0.05}Na_{0.02}K_{0.89}(Al_{0.61}Ti_{0.20}Fe_{1.25}Mn_{0.01}Mg_{0.62})(Si_{2.81}Al_{1.19})O_{10}(OH)_2$	2.70	0.75	(10a)
	$Ca_{0.05}Na_{0.02}K_{0.67}(NH_4)_{0.26}(Al_{0.56}Ti_{0.20}Fe_{1.24}Mn_{0.02}Mg_{0.61})(Si_{2.78}Al_{1.22})O_{10}(OH)_2$	2.63	0.74	(10b)
Late annite (L-Ann)	$Ca_{0.02}Na_{0.02}K_{0.89}(Al_{0.40}Ti_{0.22}Fe_{1.50}Mn_{0.01}Mg_{0.61})(Si_{2.71}Al_{1.29})O_{10}(OH)_2$	2.75	0.93	(11)

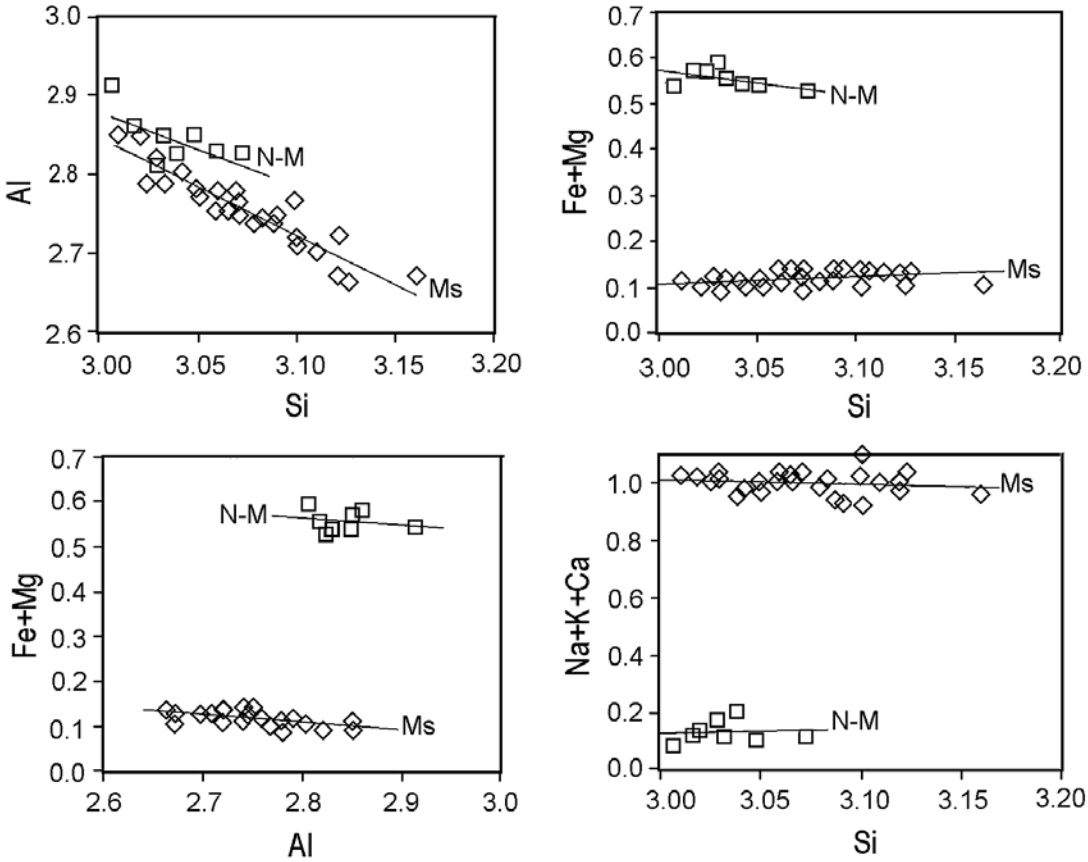

FIG. 6. Selected binary plots showing the most significant chemical characteristics of white micas from schists. Squares: ammonium-rich white mica (N–M). Diamonds: Ms (samples MP–7 and MP–8).

higher mean Al content in Ann and higher mean Fe and Mg contents in Ms lamellae (3 in Fig. 13B), relative to the Ms grain; these later differences are probably due to the presence of nanometer-scale intergrowths of Ms and Ann.

All these observations suggest that exsolution proceded through different mechanisms in the two types of grains, probably homogeneous nucleation (Ms grains) and spinodal decomposition (Ann grains). Growth of the precipitates requires, in both cases, important diffusion through the grains. It is well known that the coefficient of diffusion is variable in different crystallographic directions and that increasing temperatures and the presence of structural defects, especially vacancies, favor diffusion (Buseck *et al*. 1980, Kretz 1994). As the main chemical differences between dioctahedral and trioctahedral micas involve the Al:(Fe + Mg) ratio, an important diffusion-induced flux of these cations must have existed.

The two types of exsolution-induced microstructures can be explained on the basis of these factors. Thus, the presence of a lower number of Ann lamellae with a greater thickness in Ms grains, which contrasts with the more numerous and thinner Ms lamellae present in Ann grains, is probably due both to the different initial mechanism of exsolution and to the fact that diffusion through the Ms structure, with notably and inherent higher number of vacancies, is easier than through the Ann structure. In addition, spinodal decomposition clearly would favor the lack of well-defined crystallographic faces in Ms lamellae exsolved in Ann.

DISCUSSION

Differences in the composition of Ms and Ann from gneisses and schists and among texturally different micas (Table 7) clearly indicate that mica growth occurred at variable P–T conditions. We do not intend

to deduce a complete P–T–t path, given the numerous uncertainties related to both the attainment of equilibrium among these phases and the influence of the pre-Alpine and Alpine metamorphism. We will therefore only focus our discussion on the evolution of mica composition and on the possible temperatures of formation, based on the diagram of Monier & Robert (Fig. 14A). We will also use the geobarometer of Massone & Schreyer (1987) (Fig. 14B).

Genesis of ammonium-rich mica and exsolution lamellae

Relics of N–M, although very scarce in the Torrox area, probably provide a key for the interpretation of the evolution of micas. Tobelite formation at low temperature is related to two main geological processes: a) hydrothermal alteration of pre-existing K-mica by N-bearing fluids, and b) liberation of nitrogen during the thermal decomposition of organic matter, and fixation, as NH_4^+, in diagenetic clay minerals. During the first process, NH_4^+-for-K^+ replacement can be extensive, and almost pure tobelite can be formed in localized geological settings (Higashi 1982). In the second case, the NH_4:K ratio can be very variable, according to the amount of organic matter in or near the sediment. This process can have, in addition, a wider influence, especially in sedimentary terranes rich in organic components. As discussed previously (Ruiz Cruz & Sanz de Galdeano 2008), we believe that the more probable source of NH_4 was the organic matter initially present in the sediment, according to previous interpretations for high N contents in metamorphic rocks (*e.g.*, Itihara & Suwa 1985, Elvevold & Andersen 1993, Boyd & Philippot 1998). Indeed, the C content is high in both gneisses and schists (Table 2). With condi-

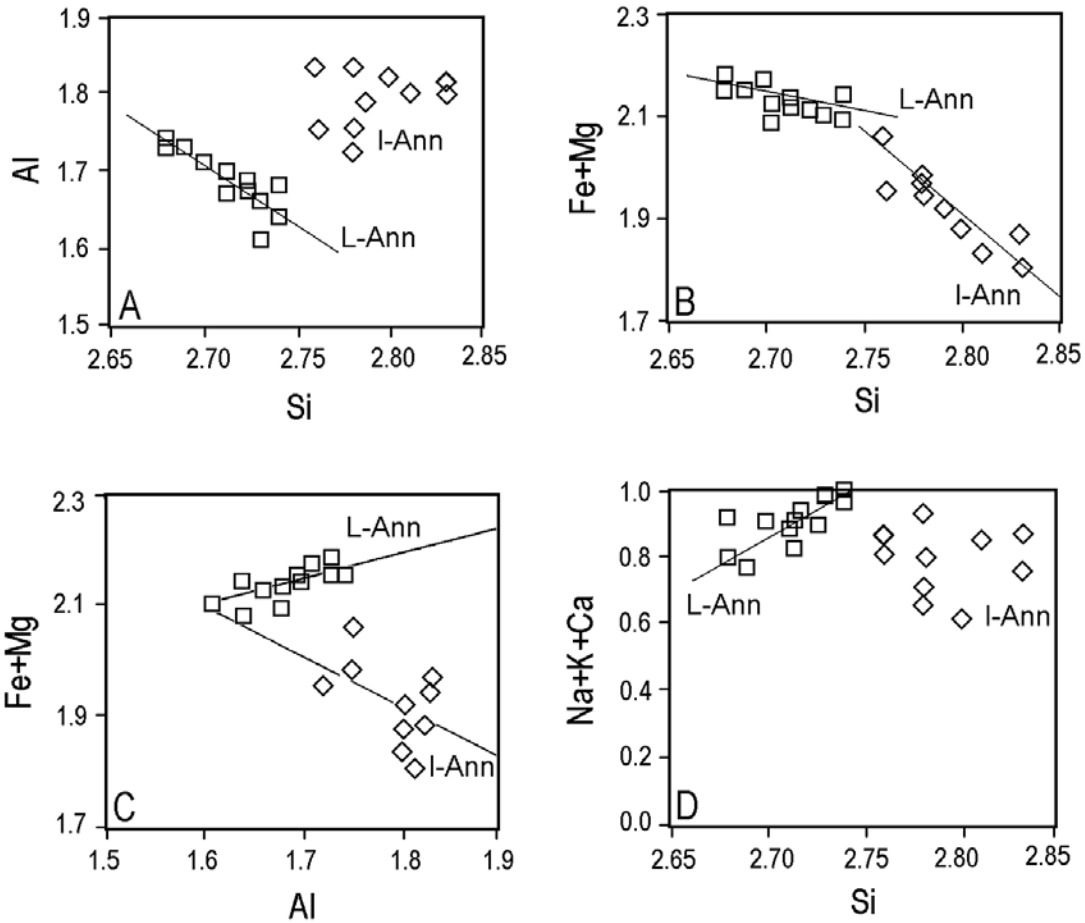

FIG. 7. Selected binary plots showing the most significant chemical characteristics of Ann from schists. Diamonds: annite grains included in kyanite. Squares: late Ann defining the main schistosity.

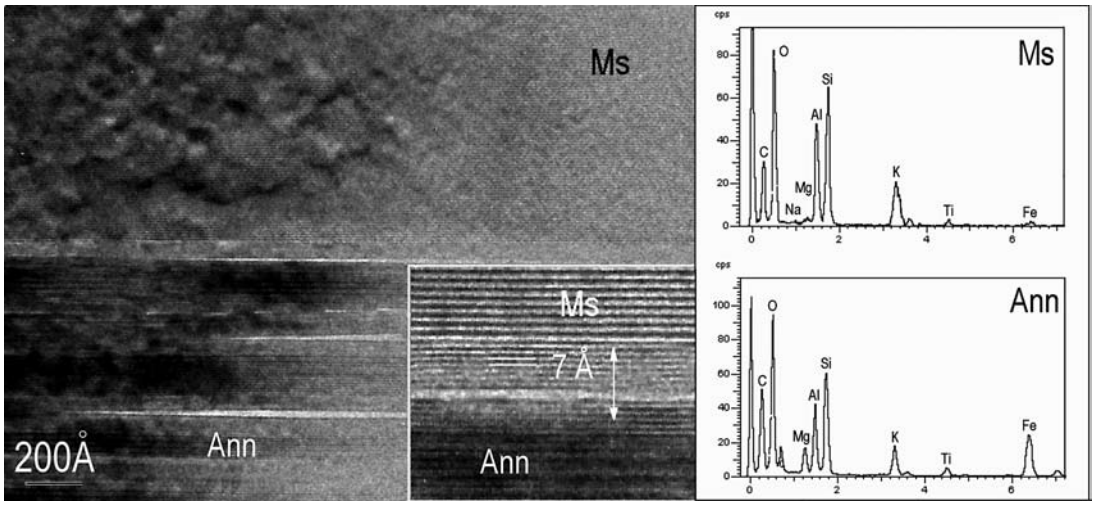

FIG. 8. Ms–Ann boundary in a Ms exsolved grain from sample MP–2. The Ms host shows apparent structural regularity, whereas the Ann lamella shows numerous structural defects. The higher-magnification image of the boundary (inset a) reveals the presence of a thin packet with 7 Å layers. Inset: EDS spectra of Ms (upper) and Ann (lower).

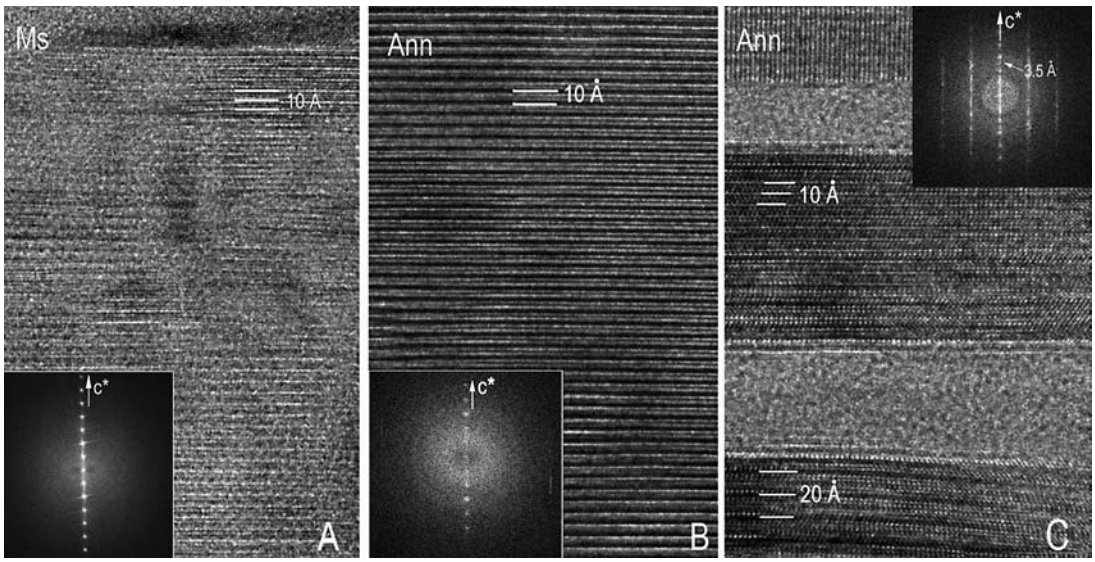

FIG. 9. Lattice-fringe images of the host Ms (A) and Ann lamellae with variable orientations (B and C) from sample MP–5. In C, areas amorphized during analysis separate the Ann packets with different orientations. This image shows the coexistence of 10- and 20-Å sequences in Ann. The Fourier transform (inset) shows the presence of 7-Å reflections.

tions of increasing metamorphism, a redistribution of ammonium between white mica and the first generation of Ann probably occurred (Sadofsky & Bebout 2000), as indicated the presence of ammonium in Ann grains included in kyanite.

The composition of N–M cannot be used to estimate temperatures from the Monier & Robert diagram because high NH_4 contents cause an unknown increase of the Fe + Mg content, which is probably not controlled only by temperature but also by crystal-chemical

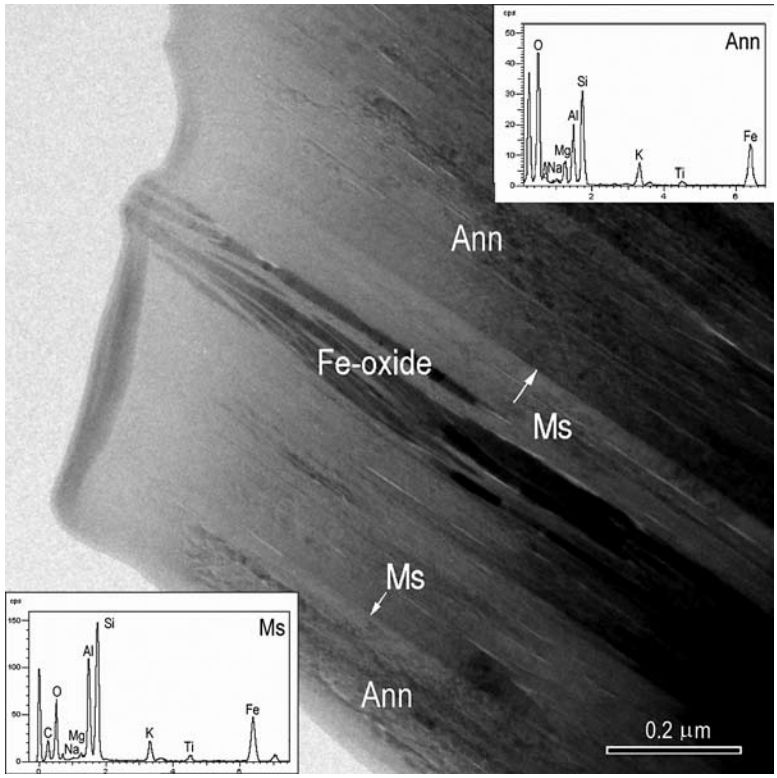

FIG. 10. Low-magnification TEM image of the boundaries between the host Ann and a Ms lamella from sample MP–2. The latter includes Fe oxide areas. Inset: EDS spectra of Ann (upper) and Ms (lower).

TABLE 8. EMPA DATA ON MICAS FROM EXSOLVED GRAINS

	1 (Ms)	2 (Ms)	3 (Ann)	4 (Ann)
SiO_2 wt.%	46.82	45.81	35.67	36.83
Al_2O_3	33.67	35.00	20.22	20.04
TiO_2	0.71	0.50	3.27	4.12
Cr_2O_3	0.02	0.03	0.04	0.03
NiO	0.00	0.00	0.03	0.06
FeO	1.13	1.02	25.39	18.73
MnO	0.00	0.03	0.18	0.13
MgO	1.09	0.73	6.01	6.98
CaO	0.02	0.03	0.48	0.21
Na_2O	0.56	0.63	1.24	0.87
K_2O	10.26	10.15	3.83	7.03
$(NH_4)_2O$	0.00	0.06	0.90	1.25
Total	94.28	93.99	97.26	96.29
Si *apfu*	3.14	3.08	2.66	2.73
^{IV}Al	0.86	0.92	1.34	1.27
^{VI}Al	1.81	1.86	0.43	0.48
Ti	0.04	0.03	0.18	0.23
Fe	0.06	0.06	1.58	1.16
Mn	0.00	0.00	0.01	0.01
Mg	0.11	0.07	0.67	0.77
Σoct	2.02	2.02	2.88	2.65
Ca	0.00	0.00	0.04	0.02
Na	0.07	0.08	0.18	0.13
K	0.88	0.87	0.36	0.66
NH_4	0.00	0.00	0.16	0.21
Σinterlayer	0.95	0.95	0.74	1.02

constraints (Guidotti & Sassi 1998). The possible Ms accompanying N–M in this first assemblage has not been identified in schists, although indirect evidence is provided by the micas from gneissic rocks.

The presence of two paragenetic types of white mica (homogeneous and exsolved primary grains) in gneisses suggests that the initial assemblage contained two inmiscible white micas, probably N–M and Ms, as is commonly observed in tobelite-bearing samples. Although N–M has not been identified in gneisses, the exsolved Ms grains were necessarily formed from a (Fe + Mg)-rich white mica with a composition similar to that of N–M, as also deduced by Ferraris *et al.* (2001).

Similarly, and although previous reports are lacking, the exsolved Ann grains must have formed from a Al-rich NH_4-bearing Ann. Mass-balance calculations are based on the observed Ms:Ann ratios in exsolved grains of Ms and Ann (2.6:1 and 1:3, respectively). The results are:

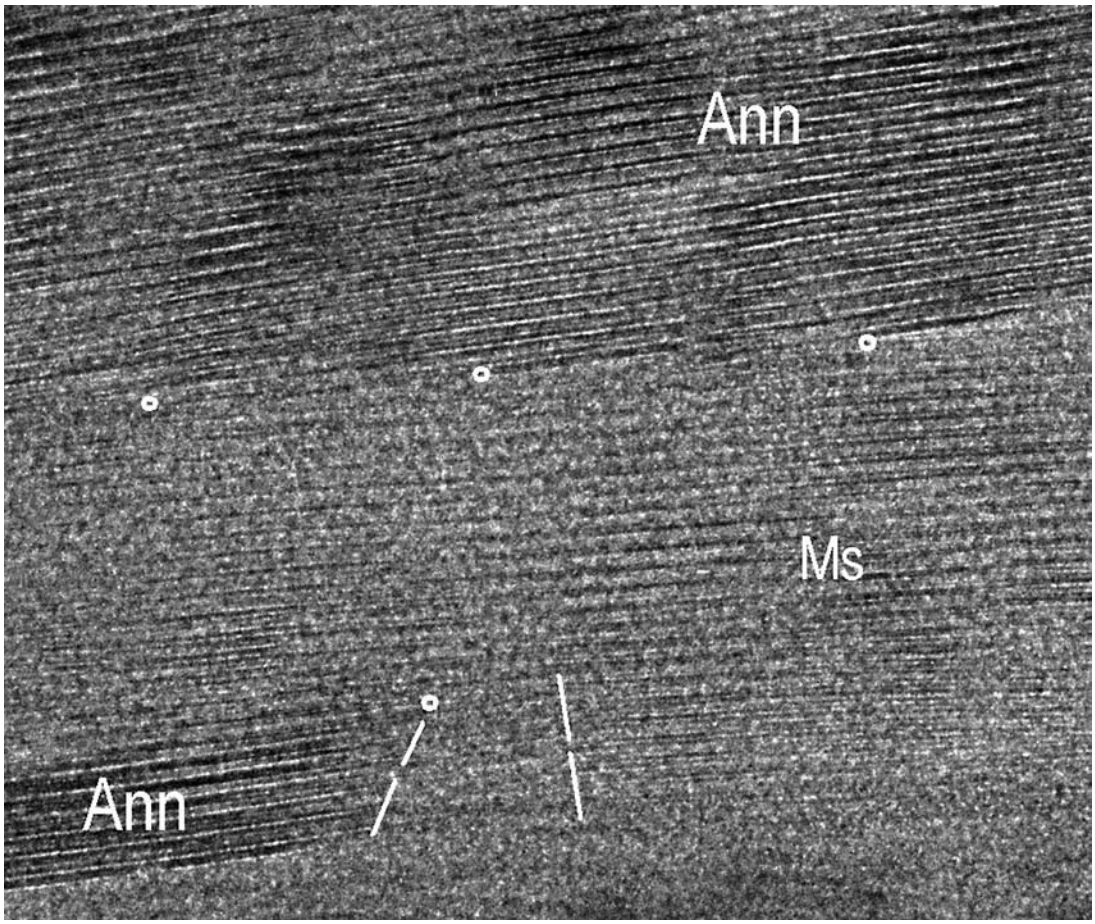

FIG. 11. Semicoherent boundaries between host Ann and Ms lamellae from sample MP–2. Small white circles mark the interface dislocations. The boundary oblique to the layers (between the white lines) appears strongly damaged.

Ms grains:

$$2.6\ [Na_{0.04}\,K_{0.96}\,(Al_{1.74}\,Ti_{0.05}\,Fe_{0.09}\,Mg_{0.12})\,(Si_{3.13}\,Al_{0.87})\,O_{10}\,(OH)_2] + 1\ [Ca_{0.02}\,Na_{0.01}\,K_{0.58}\,(NH_4)_{0.42}\,(Al_{0.42}\,Ti_{0.04}\,Fe_{1.71}\,Mg_{0.74})(Si_{2.63}\,Al_{1.37})\,O_{10}\,(OH)_2] + 0.10\ [SiO_2] \rightarrow 3.6\ [Ca_{0.005}\,Na_{0.04}\,K_{0.85}\,(NH_4)_{0.12}\,(Al_{1.40}\,Ti_{0.04}\,Fe_{0.54}\,Mg_{0.29})\,(Si_{3.02}\,Al_{0.98})\,O_{10}\,(OH)_2] \quad (1)$$

Ann grains:

$$1\ [Na_{0.01}\,K_{0.99}\,(Al_{1.70}\,Ti_{0.05}\,Fe_{0.15}\,Mg_{0.11})\,(Si_{3.18}\,Al_{0.82})\,O_{10}\,(OH)_2] + 3\ [Ca_{0.02}\,Na_{0.01}\,K_{0.50}\,(NH_4)_{0.47}\,(Al_{0.37}\,Ti_{0.04}\,Fe_{1.80}\,Mg_{0.72})\,(Si_{2.62}\,Al_{1.38})\,O_{10}\,(OH)_2] \rightarrow 4\ [Ca_{0.02}\,Na_{0.01}\,K_{0.62}\,(NH_4)_{0.35}\,(Al_{0.70}\,Ti_{0.04}\,Fe_{1.39}\,Mg_{0.57})\,(Si_{2.76}Al_{1.24})\,O_{10}\,(OH)_2] \quad (2)$$

By comparing formula 1 with formula 9b in Table 7, the main differences are related to the sheet of octahedra and the ammonium content. These differences suggest that exsolution of N–M must include the formation of some other ferromagnesian phase. Indeed, Zeck & Whitehouse (2002) described the presence of small grains of garnet associated with the exsolved Ms grains. Another possibility is that the 7-Å phase observed at the Ms–Ann boundaries also represents an exsolution product. In addition, the formation of the Ms + N–M assemblage necessarily included other reactants, as indicated by the notable increase of K in the whole grain of mica, relative to the assumed precursor N–M.

Comparison of formulae 2 and 10b (Table 7) reveals some differences, mainly affecting the sheet of octahedra. The different Ti content, higher in early N–A from schists, can be explained by the simultaneous

formation of rutile precipitates, which are very abundant in the exsolved grains of Ann. Differences in ^{VI}Al:(Fe + Mg) suggest that the Fe oxide inclusions present in the Ms lamellae (Fig. 10) also were a product of the exsolution of the ammonium-bearing annite (N–A).

A plot of the composition of the Ms host on the Monier & Robert diagram (Fig. 14A, point 1) indicates that exsolution occurred between 400 and 500°C. A similar temperature is provided by the exsolution-free grains of primary Ms (point 2 in Fig. 14A), suggesting, as the textural data, that Ms grew in equilibrium with N–M. Indeed, the existence of a miscibility gap between tobelite and Ms was already proposed by Juster *et al.* (1987) and Nieto (2002). Muscovite lamellae exsolved in Ann have slightly higher Si contents, suggesting that N–A grains exsolved at a lower temperature than N–M (point 1' in Fig. 14A).

The average Si content of Ms of this first generation (3.14 *apfu*) indicates, according to the Massone & Schreyer (1987) diagram (Fig. 14B), pressures of ~4 kbar at 450°C, which contrast with previous estimates (11–13 kbar), deduced from the maximum Si content (3.33 *apfu*) and assuming temperatures of 650°C.

According to our interpretation, the exsolution of tobelite and ammonium-bearing annite must have occurred during heating rather than during cooling, as is

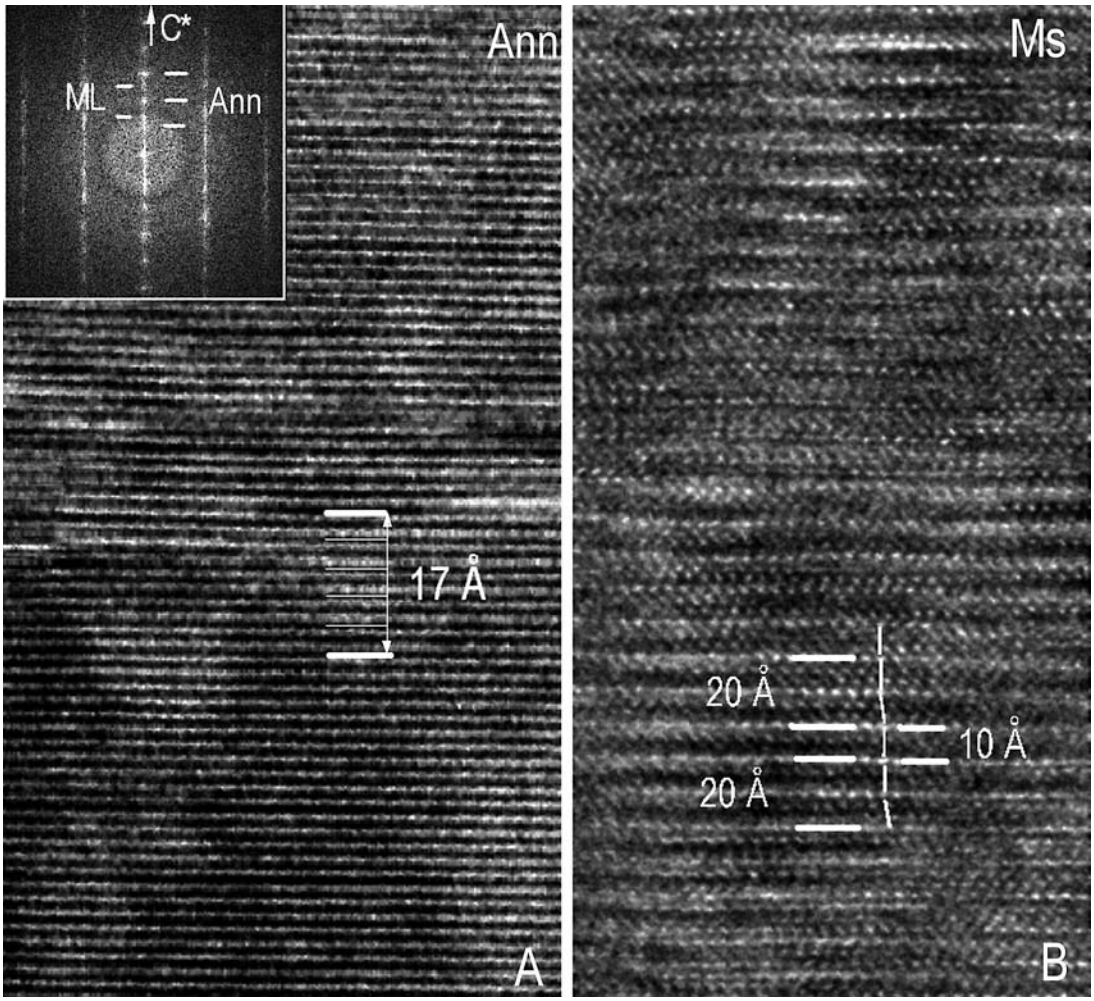

FIG. 12. A) Lattice-fringe image of Ann host, showing small areas with regular 17-Å basal spacing. The Fourier transform (inset) also shows reflections at 8.5 and 4.25 Å, corresponding to this mixed-layered structure (ML). B) A [100] zone axis high-resolution image of a Ms lamella included in Ann. Bending of layers, associated with contrast effects, prevents the accurate identification of Ms polytype, although one- and two-layer sequences are evident in some areas. Images obtained from sample MP–5.

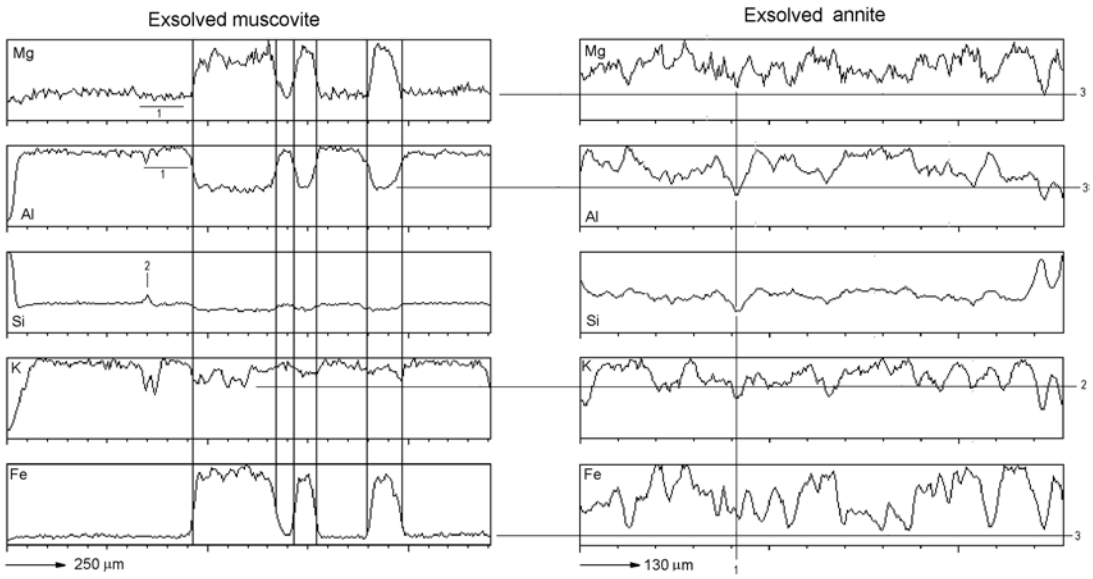

FIG. 13. Compositional profiles obtained across the exsolved grain of Ms from Figure 2B (A), and across the exsolved grain of Ann shown in Figure 2D (B).

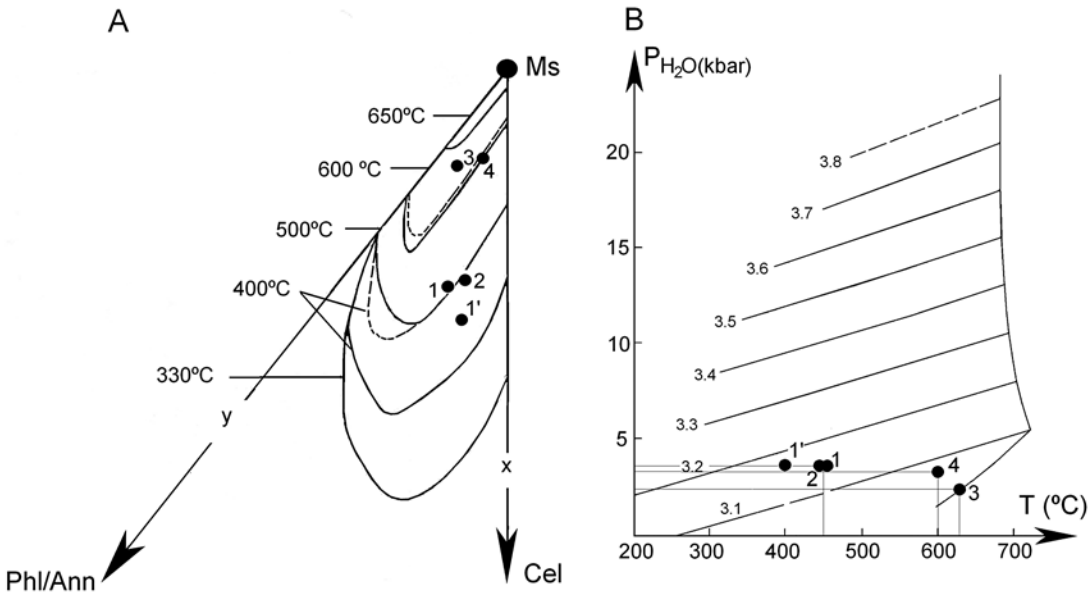

FIG. 14. A) Plot of the chemical composition of white micas from gneisses and schists on the diagram of Monier & Robert (1986). 1. Host Ms. 1'. Exsolved Ms lamellae in Ann. 2. Homogeneous primary Ms from gneisses. 3: Late Ms from gneisses. 4. Ms from schists. B) Plot of the points from Figure 14A on the diagram of Massone & Schreyer (1987).

generally observed. There are few examples of exsolution in micas, but some data support this hypothesis. For example, the experimental results of Monier & Robert (1986) indicate that at fixed pressure, the miscibility gap between di- and trioctahedral micas becomes wider at increasing temperatures. The exsolved micas described by Ferraris *et al*. (2001) were also interpreted as formed during heating, from a precursor mica with an unusual composition. It can be assumed that such precursor mica is a metastable phase, as suggested by Livi & Veblen (2004) for prograde exsolution in paragonite in Liassic shales from the Alps. Nevertheless, no data point to the metastability of tobelite from schists. In addition, no data exist about the limit of octahedral (Mg + Fe)-for-Al substitution in tobelite or annite at increasing temperatures, nor about the stability limits of these phases. In our opinion, the presence of ammonium in the interlayer must markedly influence the (Fe + Mg) solubility in the dioctahedral mica. The beginning of the release of NH_4, at increasing temperatures (~450°C according to the DTA curves available), can be a decisive factor limiting the miscibility and inducing the exsolution. Experimental data are necessary, however, to test this hypothesis.

Later micas

Late Ms grains from gneisses clearly postdate the primary grains. A plot of the average composition in Figure 14A (point 3) indicates equilibration temperatures of 625°C, notably higher than those determined for the first generation of mica. Whether this generation of mica represents the climax of the first metamorphic episode or corresponds to a second one is uncertain. The composition of Ms from schists provides slightly lower temperatures (~600°C), also higher that those deduced for the exsolution stage (Fig. 14A, point 4). In both cases, the low Si contents (3.03 and 3.07 *apfu*) indicate that this high-T event occurred at very low-P conditions (~3 kbar). Indeed, the high-P Alpine event was not preserved in the Torrox micas analyzed in this work.

Conclusions

The discovery of ammonium-rich micas in the graphite-bearing schists overlying gneisses at the Torrox area is the key to interpreting the exsolution microstructures observed in micas from the gneisses. The gneissic rocks contain two different primary white micas, homogeneous and exsolved, suggesting that the initial white-mica assemblage consisted of muscovite + ammonium-rich white mica. In addition, gneisses contain two different types of annite grains: homogeneous and exsolved, which strongly suggest that two types of annite, K- and NH_4-rich, were also present in the initial assemblage.

The presence of NH_4-enriched micas is related to the liberation of nitrogen from the organic matter during the first metamorphic episode affecting these formations. Whereas ammonium-rich micas persisted in schists, their exsolution occurred, at increasing temperature, in gneisses. The temperature of exsolution was probably in the range 400–500°C, at pressure conditions on the order of 4 kbar.

Acknowledgements

The authors are grateful to R.F. Martin, D.R. Lentz, J.V. Owen, and an unknown reviewer, whose suggestions and corrections have notably improved the manuscript. Dr. E. Puga provided detailed discussion of the manuscript and numerous suggestions. Also, we thank M.M. Abad (Universidad de Granada) and to J.L. Baldonedo and A. Gómez (Universidad Complutense) for help in obtaining TEM–AEM data, and M. Bentabol for help in obtaining the FTIR spectra. This study has received financial support from the Project CGL 2006–02481 (Ministerio de Educación y Ciencia) and from the Research Group RNM–199 (Junta de Andalucía).

References

Azañón, J.M., Crespo-Blanc, A. & Garcia-Dueñas, V. (1997): Continental collision, crustal thinning and nappe forming during the pre-Miocene evolution of the Alpujárride Complex (Alboran Domain, Betics). *J. Struct. Geol.* **19**, 1055-1071.

Azañón, J.M., Garcia-Dueñas, V. & Goffé, B. (1998): Exhumation of high-pressure metapelites and coeval crustal extension in the Alpujárride complex (Betic Cordillera). *Tectonophysics* **285**, 231- 252.

Booth-Rea, G., Azañon, J.M., Goffé, B., Vidal, O. & Martínez-Martínez, J.M.C. (2002): High-pressure, low-temperature metamorphism in Alpujárride Units of southeastern Betics (Spain). *Comptes Rendus, Série Geosciences* **334**, 857-865.

Boyd, S.R. & Philippot, P. (1998): Precambrian ammonium biogeochemistry: a study of the Moine metasediments, Scotland. *Chem. Geol.* **144**, 257-268.

Buseck, P.R., Nord, G.L. & Veblen, D.R. (1980): Subsolidus phenomena in pyroxenes. *In* Pyroxenes (C.T. Prewitt, ed.). *Rev. Mineral.* **7**, 117-211.

Busigny, V., Cartigny, P., Philippot, P. & Javoy, M. (2003): Ammonium quantification in muscovite by infrared spectroscopy. *Chem. Geol.* **198**, 21-31.

Chourabi, B. & Fripiat, J.J. (1981): Determination of tetrahedral substitution and interlayer surface heterogeneity from vibrational spectra of ammonium in smectites. *Clays Clay Minerals* **29**, 260-268.

DRITS, V.A., LINDGREEN, M.H. & SALYN, A.L. (1997): Determination of the content and distribution of fixed ammonium in illite–smectite by X-ray diffraction: application to North Sea illite–smectite. *Am. Mineral.* **82**, 79-87.

DUIT, W., JANSEN, J.B.H., VAN BREEMEN, A. & BOS, A. (1986): Ammonium micas in metamorphic rocks as exemplified by Dôme de l'Agot (France). *Am. J. Sci.* **286**, 702-732.

EGELER, C.G. & SIMONS, O.J. (1969): Sur la tectonique de la Zone Bétique (Cordillères Bétiques, Espagne). *Ver. Kon. Ned. Akad. Wet.* **25**(3).

ELVEVOLD, S. & ANDERSEN, T. (1993): Fluid evolution during metamorphism at increasing pressure: carbonic- and nitrogen-bearing fluid inclusions in granulites from Øksfjord, north Norwegian Caledonides. *Contrib. Mineral. Petrol.* **114**, 236-246.

FERRARIS, C., GROBETY, B. & WESSICKEN, R. (2001): Phlogopite exsolutions within muscovite: a first evidence for a higher-temperature re-equilibration, studied by HRTEM and AEM techniques. *Eur. J. Mineral.* **13**, 15-26.

FERROW, E.A., LONDON, D., GOODMAN, K.S. & VEBLEN, D.R. (1990): Sheet silicates of the Lawler Peak granite, Arizona: chemistry, structural variations, and exsolution. *Contrib. Mineral. Petrol.* **105**, 491-501.

FLUX, S. & CHATTERJEE, N.D. (1986): Experimental reversal of the Na–K exchange reaction between muscovite–paragonite crystalline solutions and a 2 modal aqueous (Na,K) Cl fluid. *J. Petrol.* **27**, 665-676.

FLUX, S., CHATTERJEE, N.D. & LANGER, K. (1984): Pressure-induced (Al,Si)$^{[4]}$-ordering in dioctahedral micas? *Contrib. Mineral. Petrol.* **86**, 294-297.

GARCÍA-CASCO, A., SÁNCHEZ-NAVAS, A. & TORRES-ROLDÁN, R.L. (1993): Disequilibrium decomposition and breakdown of muscovite in high P–T gneisses, Betic alpine belt (southern Spain). *Am. Mineral.* **78**, 158-177.

GHOSE, S. (1981): Subsolidus reactions and microstructures in amphiboles. *In* Amphiboles and Other Hydrous Pyriboles – Mineralogy (D.R. Veblen, ed.). *Rev. Mineral.* **9A**, 325-372.

GUIDOTTI, C.V. & SASSI, F.P. (1998): Petrogenetic significance of Na–K white mica mineralogy: recent advances for metamorphic rocks. *Eur. J. Mineral.* **10**, 815-854.

HIGASHI, S. (1982): Tobelite, a new ammonium dioctahedral mica. *Mineral. J.* **11**, 138-146.

ITIHARA, Y. & SUWA, K. (1985): Ammonium contents of biotites from Precambrian rocks in Finland: the significance of NH_4^+ as a possible chemical fossil. *Geochim. Cosmochim. Acta* **49**,145-151.

JUSTER, T.C., BROWN, P.E. & BAILEY, S.W. (1987): NH_4-bearing illite in very low grade metamorphic rocks associated with coal, northeastern Pennsylvania. *Am. Mineral.* **72**, 555-565.

KRETZ, R. (1994): *Metamorphic Crystallization*. John Wiley & Sons, Chichester, U.K.

LIVI, K.J.T. & VEBLEN, D.R. (2004): Long-range interlayer cation segregation during low-grade metamorphism of mica. *Int. Geol. Congress, 32nd* (*Florence*), *Abstr.* **1**, 307.

MARTÍN-ALGARRA, A. (1987): *Evolución geológica alpina del contacto entre las Zonas Internas y las Zonas Externas de la Cordillera Bética*. Ph.D. thesis, Universidad de Granada, Granada, Spain.

MASSONE, H.-J. & SCHREYER, W. (1987): Phengite geobarometry based on the limiting assemblage with K-feldspar, phlogopite, and quartz. *Contrib. Mineral. Petrol.* **96**, 212-224.

MINGRAM, B. & BRAÜER, K. (2001): Ammonium concentration and nitrogen isotope composition in metasedimentary rocks from different tectonometamorphic units of the European Variscan Belt. *Geochim. Cosmochim. Acta* **65**, 273-287.

MONIER, G. & ROBERT, J.-L. (1986): Muscovite solid solution in the system K_2O–MgO–FeO–Al_2O_3–SiO_2–H_2O: an experimental study at 2 kbar P_{H2O} and comparison with natural Li-free micas. *Mineral. Mag.* **50**, 257-266.

NIETO, F. (2002): Characterization of coexisting NH_4- and K-micas in very low-grade metapelites. *Am. Mineral.* **87**, 205-216.

PICHAVANT, M., KONTAK, D.J., VALENCIA HERRERA, J. & CLARK, A.H. (1988): The Miocene–Pliocene Macusani volcanics, SE Peru. *Contrib. Mineral. Petrol.* **100**, 300-324.

PUGA, E., DÍAZ DE FEDERICO, A. & NIETO, J.M. (2002): Tectonostratigraphic subdivision and petrological characterisation of the deepest complexes of the Betic zone: a review. *Geodin. Acta* **15**, 23-43.

ROBINSON, P., ROSS, M., NORD, G.L., JR., SMYTH, J.R. & JAFFE, H.W. (1977): Exsolution lamellae in augite and pigeonite: fossil indicators of lattice parameters at high temperature and pressure. *Am. Mineral.* **62**, 857-873.

ROBINSON, P., SPEAR, F.S., SCHUMACHER, J.C., LAIRD, J., KLEIN, C., EVANS, B.W. & DOOLAN, B.L. (1982): Phase relations of metamorphic amphiboles: natural occurrence and theory. *In* Amphiboles: Petrology and Experimental Phase Relations (D.R. Veblen & P.H. Ribbe, eds.). *Rev. Mineral.* **9B**, 1-227.

RUIZ CRUZ, M.D. & SANZ DE GALDEANO, C. (2008): High-temperature ammonium white mica from the Betic Cordillera (Spain). *Am. Mineral.* **93**, 977-987.

RUIZ CRUZ, M.D. & SANZ DE GALDEANO, C. (2009): Suhailite: a new ammonium trioctahedral mica. *Am. Mineral.* **94** (in press).

SADOFSKY, S.J. & BEBOUT, G.E. (2000): Ammonium partitioning and nitrogen-isotope fractionation among coexisting

micas during high-temperature fluid–rock interactions: examples from the New England Appalachians. *Geochim. Cosmochim. Acta* **64**, 2835-2849.

SANZ DE GALDEANO, C. (1997): *La Zona Interna Bético-Rifeña* (*Antecedentes, unidades tectónicas, correlaciones y bosquejo de reconstrucción paleogeográfica*). Monográfica Tierras del Sur, Universidad de Granada, Granada, Spain.

SCHROEDER, P.A. & INGALL, E.D. (1994): A method for the determination of nitrogen in clays, with application to the burial diagenesis of shales. *J. Sed. Res.* **A64**, 694-697.

SCHROEDER, P.A. & MCLAIN, A.A. (1998): Illite–smectites and the influence of burial diagenesis on the geochemical cycling of nitrogen. *Clay Mineral.* **33**, 539-546.

SHIGOROVA, T.A., KOTOV, N.V., KOTEL'NIKOVA, YE.N., SHMAKIN, B.M. & FRANK-KAMENETSKIY, V.A. (1981): Synthesis, diffractometry and IR spectroscopy of micas in the series from muscovite to the ammonium analog. *Geochem. Int.* **18**, 76-82.

VEBLEN, D.R. (1983): Exsolution and crystal chemistry of the sodium mica wonesite. *Am. Mineral.* **68**, 554-565.

ZECK, H.P. & WHITEHOUSE, M.J. (1999): Hercynian, Pan-African, Proterozoic and Archean ion-microprobe zircon ages for a Betic-Rif core complex, Alpine belt, W Mediterranean – consequences for its P–T–t path. *Contrib. Mineral. Petrol.* **134**, 134-149.

ZECK, H.P. & WHITEHOUSE, M.J. (2002): Repeated age resetting in zircons from Hercynian–Alpine polymetamorphic schists (Betic–Rif tectonic belt, S. Spain) – a U–Th ion microprobe study. *Chem. Geol.* **182**, 275-292.

Received November 27, 2007, revised manuscript accepted December 30, 2008.